

GRAPHENE SHEETS DECORATED WITH SILVER NANOPARTICLES AS AN  
OXYGEN REDUCTION REACTION CATALYST FOR ZINC-AIR BATTERY



A Thesis Submitted in Partial Fulfillment of the Requirements  
for the Degree of Master of Engineering in Chemical Engineering

Department of Chemical Engineering

Faculty of Engineering

Chulalongkorn University

Academic Year 2018

Copyright of Chulalongkorn University

แผ่นกราฟีนซึ่งตกแต่งด้วยอนุภาคเงินขนาดนาโนเมตรเป็นตัวเร่งปฏิกิริยารีดักชันของออกซิเจน  
สำหรับแบตเตอรี่สังกะสี-อากาศ



วิทยานิพนธ์นี้เป็นส่วนหนึ่งของการศึกษาตามหลักสูตรปริญญาวิศวกรรมศาสตรมหาบัณฑิต  
สาขาวิชาวิศวกรรมเคมี ภาควิชาวิศวกรรมเคมี  
คณะวิศวกรรมศาสตร์ จุฬาลงกรณ์มหาวิทยาลัย  
ปีการศึกษา 2561  
ลิขสิทธิ์ของจุฬาลงกรณ์มหาวิทยาลัย

Thesis Title	GRAPHENE SHEETS DECORATED WITH SILVER NANOPARTICLES AS AN OXYGEN REDUCTION REACTION CATALYST FOR ZINC-AIR BATTERY
By	Miss Laksanaporn Poolnapol
Field of Study	Chemical Engineering
Thesis Advisor	Associate Professor Soorathep Kheawhom, Ph.D.

---

Accepted by the Faculty of Engineering, Chulalongkorn University in Partial  
Fulfillment of the Requirement for the Master of Engineering

..... Dean of the Faculty of Engineering  
(Associate Professor Supot Teachavorasinskun, D.Eng.)

THESIS COMMITTEE

..... Chairman  
(Pimporn Ponpesh, Ph.D.)

..... Thesis Advisor  
(Associate Professor Soorathep Kheawhom, Ph.D.)

..... Examiner  
(Chalida Klaysom, Ph.D.)

..... External Examiner  
(Assistant Professor Pornchai Bumroongsri, D.Eng.)

ลักษณะพร พูลนาผล : แผ่นกราฟีนซึ่งตกแต่งด้วยอนุภาคเงินขนาดนาโนเมตรเป็นตัวเร่งปฏิกิริยารีดักชันของออกซิเจนสำหรับแบตเตอรี่สังกะสี-อากาศ. ( GRAPHENE SHEETS DECORATED WITH SILVER NANOPARTICLES AS AN OXYGEN REDUCTION REACTION CATALYST FOR ZINC-AIR BATTERY) อ.ที่ปรึกษาหลัก : รศ. ดร.สุรเทพ เขียวหอม

วิทยานิพนธ์ฉบับนี้มุ่งเน้นการพัฒนาตัวเร่งปฏิกิริยาสำหรับคาโทดของแบตเตอรี่สังกะสี-อากาศและศึกษาผลกระทบของอนุภาคนาโนเงินที่ตกแต่งบนรีดิวซ์กราฟีนออกไซด์บนคาโทดของแบตเตอรี่สังกะสีอากาศ เริ่มจากการสังเคราะห์อนุภาคนาโนเงินที่ตกแต่งบนรีดิวซ์กราฟีนออกไซด์โดยการรีดักชันด้วยน้ำตาลกลูโคสภายใต้อุณหภูมิ 60 องศาเซลเซียส จากนั้นโครงสร้างและสัณฐานวิทยาของอนุภาคนาโนเงินที่ตกแต่งบนรีดิวซ์กราฟีนออกไซด์จะตรวจสอบโดยการวิเคราะห์การกระเจิงของรังสีเอ็กซ์ (XRD) และกล้องจุลทรรศน์อิเล็กตรอนแบบส่องผ่าน (TEM) ปริมาณของโลหะเงิน (Ag) ที่อยู่ในตัวอย่างสามารถยืนยันได้จากการวิเคราะห์ EDX ตัวเร่งปฏิกิริยาที่สังเคราะห์ได้จาก 3 ความเข้มข้นนำไปสู่การหาจำนวนอิเล็กตรอนเคลื่อนย้ายซึ่งเกี่ยวข้องกับปฏิกิริยาหลักของแบตเตอรี่ โดยใช้เทคนิคอิเล็กโทรดหมุน (rotating disk electrode, RDE) และพบว่าเมื่อเพิ่มความสัดส่วนของโลหะเงินในตัวเร่งปฏิกิริยาจะให้ค่าอิเล็กตรอนเคลื่อนย้ายเพิ่มขึ้นและเข้าใกล้ 4 มากขึ้น โดยผลที่ได้แสดงให้เห็นว่าค่าความเข้มข้นที่ 0.3 โมลต่อลิตร ให้ค่าเข้าใกล้การเส้นทางการเกิดปฏิกิริยาแบบ 4 อิเล็กตรอนมากที่สุด และให้สมรรถนะของตัวเร่งปฏิกิริยาสูงที่สุดเช่นกัน ดังนั้นความเข้มข้นที่ 0.3 โมลต่อลิตร (AgNPs/rGO) จึงถูกนำมาใช้เป็นตัวเร่งปฏิกิริยาของคาโทดในแบตเตอรี่สังกะสี-อากาศ และให้ประสิทธิภาพของแบตเตอรี่ โดยมีค่าความหนาแน่นกระแสไฟฟ้า 150 มิลลิแอมป์ต่อตารางเซนติเมตร ที่ 0.435 โวลต์ และ ค่าความหนาแน่นกำลังไฟฟ้าสูงสุด 67.6 มิลลิวัตต์ต่อตารางเซนติเมตร ที่ 130 มิลลิแอมป์ต่อตารางเซนติเมตร

สาขาวิชา วิศวกรรมเคมี  
ปีการศึกษา 2561

ลายมือชื่อนิสิต .....  
ลายมือชื่อ อ.ที่ปรึกษาหลัก .....

# # 5970297821 : MAJOR CHEMICAL ENGINEERING

KEYWORD: ZINC AIR BATTERY, SILVER NANOPARTICLES, OXYGEN REDUCTION  
REACTION, REDUCED GRAPHENE OXIDE

Laksanaporn Poolnapol : GRAPHENE SHEETS DECORATED WITH SILVER  
NANOPARTICLES AS AN OXYGEN REDUCTION REACTION CATALYST FOR  
ZINC-AIR BATTERY. Advisor: Assoc. Prof. Soorathep Kheawhom, Ph.D.

The aim of this thesis is to develop a catalyst for the cathode of a zinc-air battery and to investigate the effects of reduced graphene oxide decorated with silver nanoparticles on the cathode in the zinc-air battery. First, reduced graphene oxide (AgNPs/rGO) was synthesized using glucose reduction at 60 degrees Celsius. Next, the structure and morphology of AgNPs/rGO were checked using X-ray diffraction (XRD). Then, transmission electron microscopy (TEM) analyzes were carried out. The amount of silver (Ag) decorate in graphene oxide was confirmed by EDX. Next, the synthesized catalysts at 3 concentration, using a rotating disk electrode (RDE), led to the finding of the number of electron transfer in the battery main reaction. It was noted that by increasing the concentration of Ag, the electron transfer rate increased closer to 4. Thus, the results showed that the concentration of 0.3 M gave the highest value of 4 electron pathways and the highest catalyst performance. Thereby, the concentration of 0.3 M (AgNPs/rGO) was used as the catalyst in the battery which had a current density of 150 mA / cm<sup>2</sup> at 0.435 v and a power density of 67.6 mW / cm<sup>2</sup> at 130 mA / cm<sup>2</sup>.

Field of Study: Chemical Engineering

Student's Signature .....

Academic Year: 2018

Advisor's Signature .....

## ACKNOWLEDGEMENTS

First of all, I would like to show my appreciation to my thesis advisor, Assoc. Prof. Soorathep Kheawhom, for his advice and support throughout my graduate course. His suggestion greatly improved my work and research insight. Without his assistance, the completion of this work would have been impossible.

I am gratefully acknowledged Pimporn Ponpesh, Ph.D. Chalida Klaysom, Ph.D. and Asst. Prof. Pornchai Bumroongsri, who are the thesis committee member for their comments and recommendations. I would like to thank staffs of department of chemical engineering who provide assistance to my work especially Mr.Kijchai Karnkajanaprapakul. He greatly provided technical assistance to my thesis experiment.

I would like to thank my father and mother and my sister for everything they have given to me. Without their support, life would not come this far. I would like to express my thankfulness to my friends who contributed me while I was studying in master's degree. My master's degree friend from process control and life cycle engineering laboratory have played an important role in my graduate pursuit about sharing knowledge and attitude.

จุฬาลงกรณ์มหาวิทยาลัย  
CHULALONGKORN UNIVERSITY

Laksanaporn Poolnapol

## TABLE OF CONTENTS

	Page
ABSTRACT (THAI) .....	iii
ABSTRACT (ENGLISH) .....	iv
ACKNOWLEDGEMENTS .....	v
TABLE OF CONTENTS .....	vi
1.1 Background .....	1
1.2 Objective .....	3
1.3 Scope of research .....	3
CHAPTER II THEORY .....	4
2.1 Zinc-air battery .....	4
2.1.1 Zinc electrode .....	6
2.1.2 Electrolyte .....	7
2.1.3 Separator .....	7
2.1.4 Air electrode .....	7
2.2 Electrochemical O <sub>2</sub> Reduction Reactions .....	8
2.2.1 Techniques used in electrocatalytic ORR .....	8
2.2.2 Rotating Disk Electrode (RDE) .....	9
2.2.3.2 Linear Sweep Voltammetry .....	12
2.2.4 Characterizations .....	13
CHAPTER III Literature Review .....	15
CHAPTER IV Methodology .....	19
4.1 Synthesis of Graphene Oxide (GO) .....	19

4.2 Simultaneous Reduction of Silver and Graphene Oxide.....	19
4.3 Characterization of Products.....	21
4.4 Electrochemical Characterizations.....	21
4.5 Cathode Polarization .....	23
4.6 Battery Cell Design and Fabrication .....	24
CHAPTER V Results and Discussion .....	25
5.1 Physiochemical Studies.....	25
5.2 Particle Size Analysis .....	27
5.3 Electrochemical Studies .....	29
5.5 Battery Analysis.....	38
CHAPTER VI .....	41
CONCLUSIONS .....	41
6.1 Conclusions .....	41
6.2 Recommendations and Further Studies.....	42
REFERENCES .....	43
REFERENCES .....	6
VITA.....	8



## List of Figures

<i>Figure 1 Working principle and each electrode reaction of zinc-air battery.</i> .....	5
Figure 2: Koutecky Levich Study – Voltammograms Revealing Sluggish Kinetics.....	11
Figure 3. Linear increase of the potential vs. current density.....	13
<i>Figure 4 Synthesis of graphene oxide (GO) to silver nanoparticles decorated with reduced graphene oxide (AgNPs/rGO)</i> .....	20
<i>Figure 5 Rotating disk electrode (RDE) and glassy carbon electrode (GC)</i> .....	21
<i>Figure 6 Schematic illustration of cathode polarization experiment</i> .....	23
<i>Figure 7 Schematic illustration of Zinc-air cell</i> .....	24
<i>Figure 8 Powder XRD pattern of reduced graphene oxide (rGO), graphite and graphene oxide (GO)</i> .....	25
<i>Figure 9 X-ray diffraction patterns of 0.1M AgNPs/rGO (i), 0.2M AgNPs/rGO (ii), 0.3M AgNPs/rGO (iii) and AgNPs (iv)</i> .....	26
<i>Figure 10 Transmission electron microscopies (TEM) and average size of particles for (a) 0.1M AgNPs/rGO (b) 0.2M AgNPs/rGO and (c) 0.3M AgNPs/rGO</i> .....	28
<i>Figure 11 EDX of (a) 0.1M AgNPs/rGO (b) 0.2M AgNPs/rGO and (c) 0.3M AgNPs/rGO</i> .....	29
<i>Figure 12 (A-B) Linear sweep voltammetry obtained in 0.1 M KOH saturated with O<sub>2</sub> for 0.1 M (AgNPs/rGO), 0.2 M(AgNPs/rGO): scans start at 0.1 V and scan rate 50 mV s<sup>-1</sup></i> .....	30
Figure 13 Koutecky–Levich plot. LSV obtained in 0.1 M KOH saturated .....	31
<i>Figure 14 The number of electron transfer (n)</i> .....	33
<i>Figure 15 Linear sweep voltammetry rotating disk electrode (RDE) curves of commercial 0.1M AgNPs/rGO , 0.2M AgNPs/rGO and 0.3M AgNPs/rGO in O<sub>2</sub>-saturated 0.1 M KOH with a scan rate of 50 mV s<sup>-1</sup> at 1600 rpm</i> .....	36
<i>Figure 16 Cathode polarization curve</i> .....	37
<i>Figure 17 Comparison of discharge polarization curves for performance of zinc air batteries with AgNPs/rGO and MnO<sub>2</sub> catalyst in air</i> .....	38
<i>Figure 18 Comparison of power density plots of discharge curves for performance of zinc air batteries with AgNPs/rGO and MnO<sub>2</sub> catalyst in air</i> .....	39

## List of Tables

<i>Table 1 Comparison of different types of metal-air batteries.....</i>	<i>4</i>
<i>Table 2 Thermodynamic electrode potentials of electrochemical O<sub>2</sub> reductions (17)8</i>	
<i>Table 3 The condition of cathode electrodes.....</i>	<i>23</i>
<i>Table 4 Energy dispersive x-ray spectrometry surfaces (EDX) of Ag nanoparticles of AgNPs/rGO that are prepared with different AgNO<sub>3</sub> concentrations.....</i>	<i>27</i>
<i>Table 5 the number of electron transfer at varied concentration .....</i>	<i>32</i>
<i>Table 6. A comparison of the number of electron transfer and particle size (nm) of this work with related work in the literature.....</i>	<i>34</i>
<i>Table 7 Results of current density at varied concentration of (AgNPs/rGO).....</i>	<i>35</i>
<i>Table 8 A comparison of zinc-air battery performance in this work with related work in the literature.....</i>	<i>40</i>

# CHAPTER I

## INTRODUCTION

### 1.1 Background

Electricity is a most important and convenient way of energy consumption. Electricity is clean and exhibits high efficiency (1, 2). Electrical appliances require minimal maintenance and produce small environmental impacts. Specifically, electrification of transportation is significant for long-term carbon reduction goals and offers broad societal benefits (3). In Thailand, transportation is a large sector of the economy and contributes up to 55% of energy consumption. Thus, electrification will remarkably increase the sustainability and energy security of the country, as well as reduce environmental impacts.

An essential element for electrification of transportation is electrical energy storage systems (EES). The most common kind of EES is the use of a battery. Lithium-ion batteries (LIBs) have been the most widely recognized EES devices employed in various applications. Unfortunately, their limitations, such as high cost and safety issues, are the primary barrier to their successful implementation. Besides, lithium (Li) supply, as well as its future production, is far from adequate for use in the transportation sector. The distribution of Li is limited (4). For instance, a significant quantity of Li is found only in the Andes and Tibet. However, other mature technologies based on nickel (Ni) such as nickel-metal hydride (NiMH) and sodium nickel chloride (NaNiCl) batteries can be employed. Yet, Ni too is expensive and produced in relatively limited quantities. These technologies are affected by their nickel requirements for production in large quantities (5).

Zinc-air batteries (ZABs) have exhibited high potential for various energy applications because of their very high energy densities (1.35 kWh/kg) at low cost. Besides, zinc (Zn) is an attractive anode material because it is lightweight, non-toxic, inherently safe, inexpensive and abundant (4). Zinc is also the metal produced in the fourth largest quantity after iron (Fe), copper (Cu), and aluminum (Al). An established

Zn recycling industry exists to reclaim Zn from its myriad uses in industry. Moreover, Zn has widespread accessibility and availability throughout the world (6).

The mechanism behind ZABs involves Zn dissolution at the anode and oxygen reduction reaction (ORR) at the cathode. The performance of the cathode has a decisive impact on the performance of ZABs because the sluggish ORR kinetics increase overpotential and decrease power density as well as the performance of ZABs (6). The mechanism of ORR is complicated and involves many intermediates depending on the characteristics of the cathode, catalyst and electrolyte. Various research works have been carried out for developing electrocatalysts to reduce overpotential and enhance the performance of ZABs. In aqueous solutions, the ORR can proceed via two pathways: a direct four-electron pathway and a peroxide two-electron pathway. In the direct four-electron pathway, oxygen directly reduces to  $\text{OH}^-$ . In the peroxide two-electron pathway, an initial reduction to  $\text{HO}_2^-$  is followed by the reduction of  $\text{HO}_2^-$  to  $\text{OH}^-$ . The peroxide pathway of the ORR is more common in alkaline solutions, and the direct four-electron pathway of the ORR proceeds by dissociative absorption on the metal catalyst surface (7).

An efficient, durable and low-cost air cathode with low polarization ORR is essential for high performance and a long life zinc-air battery. Noble metals and transition-metal oxides are commonly used as ORR catalysts (8). However, high cost, scarcity, and inferior durability of noble metals prevent their practical applications. In contrast, ORR catalysts that are based on earth's abundant elements have been recently recognized as a new class of low-cost and environmentally benign electrocatalysts.

Platinum (Pt) is known to be the best electrocatalyst for ORR in alkaline fuel cell cathodes but its cost is high. Thus, Non-Pt catalysts based on metals such as Au (9), Pd (10) and Ag need to be developed. Silver is a good candidate because it is significantly cheaper than the others and thermodynamically and electrochemically stable at high pH, with high activities in ORR in alkaline medium (11).

Graphene is a 2D monolayer of carbon atoms densely packed in a honeycomb crystal lattice. Graphene has attracted tremendous attention as a promising material for next-generation energy storage devices because of its superior properties (12). Graphene exhibits a unique two-fold advantage with remarkably high electron mobility at room temperature and fast heterogeneous electron transfer at the edges. Besides, graphene has an ultrahigh surface area of  $2630 \text{ m}^2\text{g}^{-1}$ , which is significantly higher than its 1D counterparts i.e. ( carbon nanotube,  $1315 \text{ m}^2\text{g}^{-1}$ ) and 3D (graphite,  $10 \text{ m}^2 \text{ g}^{-1}$ ) (13). Recently, graphene has obtained much attention as regards decoration with metal nanoparticles. Synthesis of silver nanoparticles on graphene has been reported. Actually, graphene when decorated with silver nanoparticles exhibited superior electronic, ionic conductivity, and good ORR performance (14).

## 1.2 Objective

The aim of this work is to develop a cathode electrode for zinc-air batteries and to investigate the effects of reduced graphene oxide decorated with silver nanoparticles on the cathode side of a zinc-air battery.

## 1.3 Scope of research

This work consists of synthesizing reduced graphene oxide (rGO) decorated with silver nanoparticles (AgNPs). First, silver nitrate ( $\text{AgNO}_3$ ) was mixed together with graphene oxide; the various concentration of silver nitrate were added i.e. 0.1M, 0.2M and 0.3M for synthesizing AgNPs/rGO. Next, the synthesized AgNPs/rGO was analyzed in order to check oxygen reduction reaction (ORR) activity using a rotating disk electrode (RDE). Then, the AgNPs/rGO was fabricated on the cathode side of the zinc-air battery in order to check the performance of the battery.

## CHAPTER II

### THEORY

#### 2.1 Zinc-air battery

A battery is a device that is used to store energy for many portable devices, such as mobile phones, tablets, cameras, hearing aids etc (8). Currently, the demand for batteries is increasing but batteries still have some problems regarding environmental and safety use. A lithium-ion battery, for example, that is commonly used today, is a flammable battery. Further, lead -acid batteries have high toxicity. In recent years, metal-based batteries have gained a lot of attention, especially zinc-air batteries (Zn-air). Zinc-air batteries are noted to be a safety-critical battery for future device applications. Table 2.1 represents Zn-air batteries. Zn-air batteries have a higher energy density than Fe-air and K-air batteries, while magnesium air (Mg-air) and lithium-air (Li-air) batteries have higher energy densities than zinc-air batteries (Zn-air). However, magnesium-air (Mg-air) and lithium-air (Li-air) batteries do not meet safety and cost requirements. Therefore, zinc-air batteries have a high potential for future application (9).

Table 1 Comparison of different types of metal-air batteries

Types of batteries	Fe-air	K-air	Zn-air	Mg-air	Li-air
Theoretical energy density (Wh kg <sup>-1</sup> )	763	935	1,086	2,840	3,458
Practical energy density (Wh kg <sup>-1</sup> )	60-80	n/a	350-500	400-700	45-80
Cost of metal (\$)	0.40	~20	1.85	2.75	68

Zinc-air cells are composed of three parts i.e. zinc metal as an anode, an air electrode as the cathode, which is divided into a gas diffusion layer and a catalytic active layer, and a separator, as shown in Figure 1. (15):

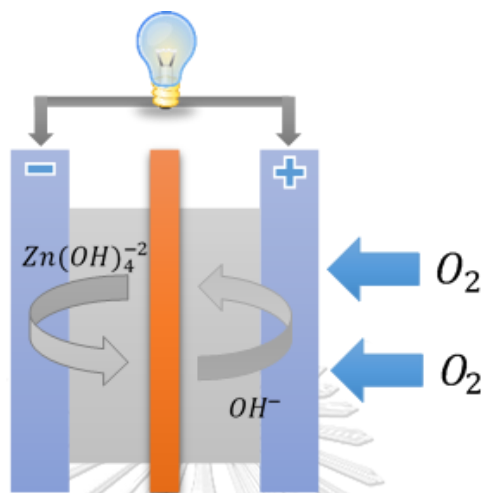


Figure 1 Working principle and each electrode reaction of zinc-air battery.

During battery discharge, zinc is oxidized into soluble zincate ions ( $\text{Zn(OH)}_4^{2-}$ ). This reaction usually proceeds until they are supersaturated in the electrolyte, after which the zincate ions decompose to insoluble zinc oxide, as shown below by the following equations:

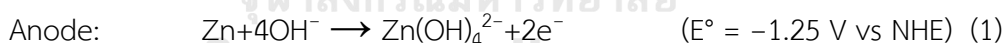


Figure 1. At the anode, zinc is oxidized with hydroxide ions. Then, it transforms into zincate ion, as expressed in Eq. 1. Zincate ion remains in the solution until supersaturation limit and then transforms into zinc oxide and water, as expressed in Eq. 2. At the cathode, oxygen is reduced with electrons and water; it then transforms into hydroxide ions, as expressed in Eq. 3. The overall reaction can

be expressed as in Eq. 4. Theoretically, the standard cell potential of ZAFC is 1.65 volt.

The practical voltage of an actual zinc-air cell is much smaller than 1.65V. It is noted that the overpotential at the zinc anode is relatively smaller than that at the air electrode. As a result, many studies have focused on how to minimize the large overpotential in the cathode reaction by developing new catalysts and modifying air electrode structures. Optimizing electrocatalytic activity is a matter of achieving the highest possible current at the lowest possible overpotential. For rechargeable zinc-air batteries, electrochemical reactions are not reverted until a large charging voltage of about 2.0 V or higher is applied. Significant deviation of both charge and discharge voltages from the equilibrium value are mostly contributed by the substantial overpotentials of oxygen electrocatalysis at the positive electrode (8).

### 2.1.1 Zinc electrode

Zinc possesses a unique set of attributes including low equivalent weight, reversibility, high specific energy density, abundance and low toxicity. Zinc is a most electropositive metal that is relatively stable in aqueous and alkaline media without significant corrosion. During discharge, zinc metal participates in anode reaction. The most practical method of improving the performance of the zinc anode is to increase the surface area of the zinc particles so that the zinc can react with the alkaline electrolyte more efficiently (14).

However, as the electrode surface area increases, the corrosion rate of zinc electrode generally becomes more significant (7). The gradual self-corrosion of zinc metal is caused by parasitic hydrogen evolution reaction. Einerhand et al. used a rotating ring disk electrode (RRDE) to determine the amount of hydrogen produced from the electrodeposition of zinc in alkaline solution and showed that hydrogen evolution increased with decreasing concentration of potassium hydroxide (KOH) and zincate ( $\text{Zn(OH)}_4^{2-}$ ) (15). In addition, in batteries, zinc changes structure and shape during repeated charge/discharge cycles, corresponding to zinc dissolution and



redeposition on the current collector. The typical shape change problems that have been reported are dendrite formation and electrode densification.

### 2.1.2 Electrolyte

Zinc-air batteries operate in alkaline media. Air works in an electrolyte with a base such as potassium hydrogen peroxide (KOH) and sodium hydroxide (NaOH). These solutions are often used in research. Potassium hydroxide is used mostly since the conductivity of potassium ion is higher than sodium ion. Potassium hydroxide is often used because of its good ionization, higher oxygen diffusion coefficient, and lower viscosity (16). It is used most commonly at concentration of 7M to 9M.

### 2.1.3 Separator

The role of a separator is to keep apart the positive and negative electrodes. It is an electrochemically inactive component. Separators for zinc-air batteries must have a low ionic resistance and high electrical resistance. They should have a high adsorption capacity of the alkaline electrolyte and sufficient chemical resistance against the corrosive electrolyte and oxidation (9).

### 2.1.4 Air electrode

ORR mainly occurs at the triple phase boundary where the electrode is in close contact with an electrolyte and the gas phase. An air electrode requires to be a proper catalyst having a highly porous structure. In zinc-air batteries, air electrodes should be capable of catalyzing both the ORR and OER efficiently. This can be achieved either by using combinations of functional components or by employing a bifunctional oxygen catalyst that can fulfill both roles. These electrocatalysts include noble metals and alloys, carbon materials, quinone and derivatives, transition metal macrocyclic compounds, transition metal chalcogenides, and transition metal carbides (2).

## 2.2 Electrochemical O<sub>2</sub> Reduction Reactions

Alkaline electrolytes are commonly used in aqueous electrolytes because oxygen reduction reaction (ORR) is more favorable in alkaline electrolytes. The aqueous electrolytes that are most commonly used in zinc air batteries are potassium hydroxide, sodium chloride, brine solution and saline solution.

### 2.2.1 Techniques used in electrocatalytic ORR

Rotating disk electrode (RDE) techniques are mostly used to study kinetics and the mechanism of oxygen electrode reactions. The rotating disk electrode (RDE) technique is a powerful tool for evaluating the activity of oxygen electrode reaction. It is used frequently in electrocatalytic ORR. RDE is a convection electrode system and consists of a disk of electrode and rotating shaft. In this research, three non-electrochemical kinetic parameters, such as the kinematic viscosity of electrolyte solution, diffusion coefficient of oxygen as well as solubility of oxygen were investigated for rotating disk electrode. (17)

Table 2 Thermodynamic electrode potentials of electrochemical O<sub>2</sub> reductions (17)

Electrolyte	ORR reactions	Thermodynamic electrode potential at standard condition, V
Alkaline aqueous solution ( Four- electron pathway)	$O_2 + 2H_2O + 4e^- \rightarrow 4OH^-$	0.401
Alkaline aqueous solution ( Two- electron pathway)	$O_2 + H_2O + 2e^- \rightarrow HO_2^- + OH^-$ $H_2O + HO_2^- + 2e^- \rightarrow 3OH^-$	-0.065 0.867

### 2.2.2 Rotating Disk Electrode (RDE)

RDE specialized hydrodynamic electrode used in the study of the kinetics and mechanism of electrode reaction

- Well-defined hydrodynamics flow to electrode surface.
- The mathematical equations are available for the calculation of different parameters.
- Rate of material transport depends in a well-defined manner on the rotation speed of the electrode.
- Systems with RDE are relatively simple for fabrication and operation.

The current measured from RDE is described by Koutecky-Levich equation:

$$\frac{1}{i} = \frac{1}{i_k} + \frac{1}{i_L}$$

Where  $i$  is the disk current density,  $i_k$  is the kinetic current density, and  $i_L$  is the Levich current density. Koutecky-Levich equation determines the  $n$ -values (from the slopes) and rate constants (from the intercepts). The diffusion-limited steady current density ( $i_L$ ) is related to the velocity of RDE ( $\omega = \text{rpm}$ ),  $m$  being the frequency in revolution per minutes) by Levich equation:

$$i_L = 0.201nFAC_{O_2}D_{O_2}^{2/3}v^{-1/6}\omega^{1/2}$$

However, electron-transfer controls the rate of the ORR: reaction is mixed control. Herein, Koutecky-Levich equation is as follows:

$$\frac{1}{i} = \frac{1}{i_k} + \frac{1}{0.201nFAC_{O_2}D_{O_2}^{2/3}v^{-1/6}\omega^{1/2}}$$

The Koutecky-Levich Equation :  $F$  is Faraday constant ,  $A$  ( $cm^2$ ) is the electrode area,  $C_{O_2}$  is the concentration of dissolved  $O_2$  in  $mol/L$  0.1M KOH solution at  $25^\circ C$   $D_{O_2}$

( $\text{cm}_2\text{s}^{-1}$ ) is diffusion coefficient of  $\text{O}_2$ ,  $\nu$  ( $\text{cm}_2\text{s}^{-1}$ ) is kinematic viscosity of the electrolyte solution and  $\omega$  ( $\text{rpm}$ ) is the rotation rate represented by rpm. Where  $I$  is the disk current density,  $i_k$  is the kinetic current density, and  $i_L$  is the Levich current density, where  $n$  ( $\text{mol}^{-1}$ ) is the overall electron transfer number.

### 2.2.3.1 Koutecky-Levich Analysis

When the rate of a half reaction occurring at an electrode surface is limited by a combination of mass transport and sluggish kinetics, it is often possible to use a rotating disk electrode to elucidate both the mass transport parameters and the kinetic parameters from a properly designed Levich study. A full treatment of this kind of analysis is beyond the scope of this document, but the following is a general description of how to extract kinetic information from a set of rotating disk voltammograms.

When the electron transfer process at an electrode surface exhibits sluggish kinetics, the voltammogram appears stretched out along the potential axis and the shape of the sigmoidal wave is slightly distorted. Comparing a set of voltammograms with facile kinetics with a set of voltammograms with sluggish kinetics Fig.7, the mass transport limited current (marked by red circles in each figure) is shifted from the standard electrode potential when there are slow kinetics. Stated another way, when a sluggish redox half reaction is studied with a rotating disk electrode, a larger overpotential must be applied to the electrode to overcome the sluggish kinetics and reach the mass transport limited current. (18)

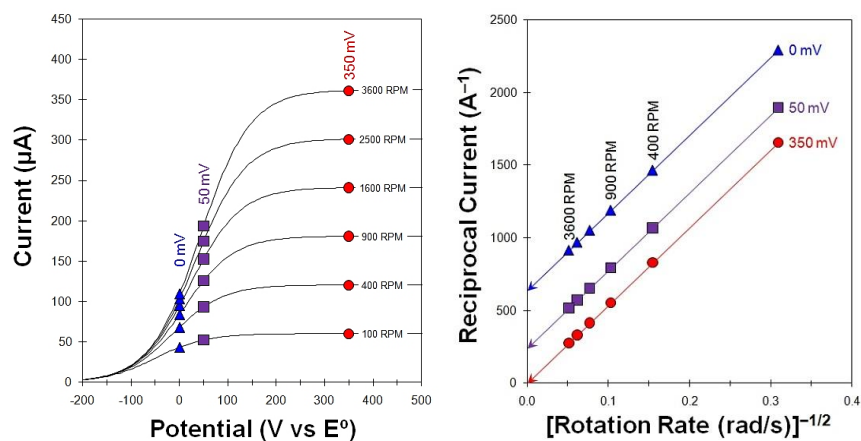


Figure 2: Koutecky Levich Study – Voltammograms Revealing Sluggish Kinetics

The general approach is to acquire a set of voltammograms at different rotation rates (i.e., perform a Levich study) and then plot the reciprocal current on a Koutecky-Levich Plot. In the example provided (Fig.3, left), the current was sampled at two locations along the rising portion of the voltammograms, marked with blue triangles and purple squares) and at one location on the limiting current plateau. A linear relationship is evident (Fig.3, right) when these sampled currents are plotted on a Koutecky-Levich plot.

For the set of currents sampled on the limiting current plateau (red circles), an extrapolation back to the vertical axis (i.e., to infinite rotation rate) yields a zero intercept. This is the identical result obtained for a facile half-reaction (see Fig.3, right) because these currents are sampled at a high enough overpotential that there are no kinetic limitations. Only mass transport limits the current, and the usual Levich behavior applies.

However, for the two sets of currents sampled on the rising portion of the voltammogram (see Fig.3, blue triangles and purple squares), the extrapolation back to the vertical axis yields non-zero intercepts. This non-zero intercept indicates a kinetic limitation, meaning that even if mass transport were infinite, the rate of the half-reaction would still be limited by the slow kinetics at the electrode surface. The

linear portion of the data on a Koutecky-Levich plot is described by the Koutecky-Levich equation (below).

$$\frac{1}{i} = \frac{1}{i_k} + \left( \frac{1}{0.201nAF C_{O_2} D_{O_2}^{2/3} \nu^{-1/6}} \right) \omega^{-1/2}$$

Plotting the reciprocal current ( $1/i$ ) against the reciprocal square root of the angular rotation rate ( $\omega^{-1/2}$ ) yields a straight line with an intercept equal to the reciprocal kinetic current ( $1/i_k$ ). The kinetic current is the current that would be observed in the absence of any mass transport limitations. By measuring the kinetic current at a variety of different overpotentials along the voltammogram, it is possible to determine the standard rate constant for the electrochemical half reaction.

### 2.2.3.2 Linear Sweep Voltammetry

Linear sweep voltammetry (LSV) is the most common form of voltammetry. When working in the context of electroanalytical chemistry with a non-rotating electrode, this technique is known as linear sweep voltammetry. LSV involves sweeping the electrode potential from an initial value to a final value at a constant rate. Linear sweep voltammetry depends on a number of factors including:

- The rate of the electron transfer reaction(s)
- The chemical reactivity of the electroactive species
- The voltage scan rate

In LSV measurements the current response is plotted as a function of voltage rather than time, unlike potential step measurements. . The voltage is scanned from a lower limit to an upper limit.

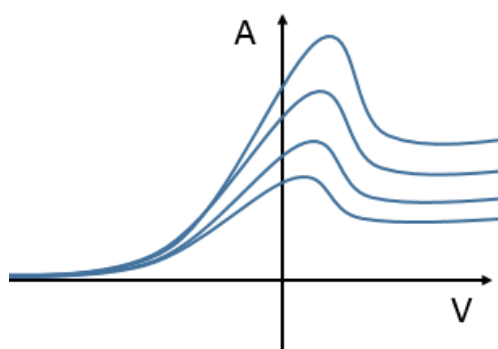


Figure 3. Linear increase of the potential vs. current density.

## 2.2.4 Characterizations

### X-ray Powder Diffraction (XRD)

X-ray diffraction is a characterization tool which identifies chemical crystalline material of an unknown substance in chemistry. It also identifies minerals and inorganic compounds in the material science field. XRD uses the interaction of the incident rays with the sample to determine the atomic and molecular structure of an unknown material. In this research, XRD technology helps to analyze the structural properties of nanomaterial (16):

- Graphene oxide (GO)  $2\theta$  has a value of 24.1.
- Graphite  $2\theta$  has a value of 25.2.
- Reduced graphene oxide (rGO)  $2\theta$  has a value of 10.2
- Silver Nanoparticles (AgNPs)  $2\theta$  have values of 38.1, 44.3, and 64.4

### Transmission Electron Microscope (TEM)

Transmission electron microscope is a characterization tool used to study thin samples as well as to study details of internal components. Through the employment of TEM, the opportunity to study the size of silver nanoparticles decorated on a graphene sheet is possible. Therefore, TEM was used to study the size of silver nanoparticles decorated on graphene sheets for the sample (AgNPs/rGO).

### Field Emission Scanning Electron Microscopy (FESEM)

Field emission scanning electron microscopy FESEM is a characterization tool used to investigate molecular surface structures. FESEM is a scanning electron microscope with magnification of up to a million times. Thus, FESEM provided the surface structures as shown in Fig.10.





## CHAPTER III

### Literature Review

Tang, X.-Z., et al. (19) demonstrated the synthesis of graphene decorated with silver nanoparticles by simultaneous reduction of graphene oxide (GO) together with silver ions with glucose as the reducing agent and polyvinylpyrrolidone as the surface modifier. By comparing the different reduction efficiencies of the samples GO and rGO, under a different temperature, it was realized that the addition of both glucose and a silver–ammonia solution enabled a good dispersion of GO for the decoration of graphene with silver nanoparticles.

Kumar et al. (20) synthesized silver nanoparticles decorated on reduced graphene oxide and examined the ORR catalytic performance of Ag/rGO for rechargeable lithium-air batteries. Stable capacity was observed for about 30 cycles. It was noted that, when ethylene glycol was used as a reducing agent, it brought about the synthesis of reduced graphene oxide with silver nanoparticles i.e. (Ag/rGO). The results indicated that Ag/rGO was a promising catalyst for rechargeable lithium-air batteries. This could also be a promising catalyst for rechargeable zinc-air batteries as well.

Over the last few years, electrical rechargeable zinc-air batteries have received attention as regards the improvement of bifunctional catalysts. Most studies have focused on cobalt, nickel, and manganese in the form of either alloys or oxides because of the relatively lower costs than noble metals. Among noble metals, silver shows an ORR activity close to that of Pt but has a much lower price. Silver nanoparticles have been extensively decorated on carbon substrate such as graphene oxide (21) and graphene (14).

Lim, E. J. et al. (21) reported Ag nanoparticles were successfully obtained on reduced graphene oxide (RGO) through the simultaneous reduction of Ag and graphene oxide (GO) without surfactant by controlling growth of Ag nanoparticles at low temperatures. Thus, the sample (Ag/RGO) improved ORR activity by changing the potential half-wave towards more positive values and increased mass activity via a 4-electron transfer pathway under alkaline conditions in the ORR process. These results suggest that providing a small particle size with a good catalyst and RGO may give good electrocatalyst support.

Lopes and Joao (14) stated that the high quality graphene metal nanoparticles composite with oxidation at low degree were put in order by a surfactant which assisted electrochemical exfoliation. A double pulse technique was used for Ag decoration of graphene (Ag/rGO) to control the size of nanoparticles. This method was able to prepare graphene resulting in a good performance of ORR.

Soo et al. (22) noted that the way to prepare a non-Pt metal catalyst (Ag/N-rGO) was to use metal salts with graphite oxide and melamine with a simple thermal annealing. The Ag/N-rGO RRDE results demonstrated onset potential and a limiting diffusion current density with four-electron pathway. The highest catalytic activity of Ag/N-rGO was accredited to the integration of the electrochemical activity of the dispersed Ag nanoparticles supported on the N-rGO surface and the unique properties of N-rGO. Even though the onset potential of Ag/N-rGO was lower than 20% of Pt/C, the current density limitation as well as a number of electron transfer were able to be compared with Pt/C. Therefore, these electrochemical results can be recommended such that Ag/N-rGO has the potential to substitute the Pt/C catalyst for ORR in alkaline media because of lower costs and the good catalytic activity of ORR.

Soorathep and Sira (1) found that a screen-printing technique was inexpensive, eco-friendly, simple and highly productive. They fabricated a zinc-air battery using

inexpensive screen-printing nano-silver ink on a polyethylene terephthalate (PET) substrate and a polypropylene (PP) membrane. Further, carbon black ink, PTFE powder, styrene butadiene binder, toluene as the solvent ( $\text{CeO}_2$ ) and catalysts ( $\text{MnO}_2$ ) were screen-printed directly onto the cathode side. The results of the discharge potential at the current density of  $5\text{mA}/\text{cm}^2$  were found to be approximately 0.25V higher than the battery without metal oxides.

Xu, Ivey et al. (23) recorded that a zinc-air system consisted of alkaline electrolytes. Moreover, potassium hydroxide (KOH) was the most commonly used alkaline because of its high conductivity, high activity and good low temperature performance. In many studies, 7 to 9 M KOH was selected because hydroxide ion had good conductivity and high concentration. This suggested that electrolyte conductivity played an important role in zinc air fuel cell (ZAFC). Improvement of the electrolyte conductivity was seen as a promising solution to enhance ZAFC performance.

In the literature, studies on graphene decorated with silver nanoparticles in zinc-air batteries have hardly been reported. However, studies of silver nanoparticles with carbon-based materials like carbon nanotubes can be found.

Wang et al. (24) synthesized silver nanoparticles decorated on single-walled carbon nanotubes in bifunctional gas diffusion electrodes for zinc-air batteries. The SWNT networks provided a highly porous surface for active oxygen absorption and diffusion. The high conductivity of SWNTs, coupled with the catalytic activity of AgNPs for oxygen reduction, pointed to an improvement in the performance of the zinc-air cell. Among the AgNPs-SWNT GDEs, the smallest particle size was seen to be favorable over the other particle sizes investigated.

Cui et al. (25) reported a new method for manufacturing ammonia sensors using AgNPs decorated RGO hybrid nanostructures in a simple and controlled fashion. The RGO/Ag hybrid sensors demonstrated higher sensitivity as compared to RGO

alone. The fast response enabled the silver nanoparticles (AgNPs) decoration on RGO to be obtained.

Wang et al. (26) prepared silver to decorate nitrogen-doped carbon sheets (Ag/NC) using a facile and in-situ thermal treatment. The Ag/NC demonstrated outstanding ORR activity in contrast to NC. This good performance was accredited to the synergistic effect between N species and Ag particles and the more pyridinic N species. Moreover, when Ag/NC and Pt/C were compared, Ag/NC showed better methanol tolerance and stability. Thus, it was seen that Ag/NC could be used to substitute Pt-based catalysts in alkaline media.

Guo et al. (27) used a citrate-protecting method in order to prepare four different metal loading Ag/C catalysts. The factors that had an effect on the Ag/C activity in ORRs were found in alkaline solutions. The ORRs on Ag/C catalysts were investigated via 4-electron pathway. Thus, when metal loading was increased, peak intensity increased directly and the ORR onset potential shifted positively with Ag loading reaching upwards, from (10 to 60) wt %.

Amanda C. (28) reported that glycerol, when used as a reducing chemical in alkaline conditions, can generate colloidal and carbon-supported AgNPs. The nanosized nature of the silver particles gave a maximum UV-vis spectrum as confirmed by using TEM images. The number of electron transfer of Ag/C was 2.7 electrons per O<sub>2</sub>. This process can be improved by optimizing the process of synthesis. The glycerol method since it is simple, inexpensive, and environmentally friendly, should be carefully considered as a routine way to produce Ag nanoparticles.

## CHAPTER IV

### Methodology

#### Experimental Procedures

##### 4.1 Synthesis of Graphene Oxide (GO)

Synthesis involves both oxidation and exfoliation of graphite sheets. Graphene oxide is prepared by oxidation of natural graphite powder using a modified Hummer method. Graphite powder (2 g) and  $\text{NaNO}_3$  (2 g) were mixed together with 90 mL of  $\text{H}_2\text{SO}_4$  (98%) in a 1000 ml volumetric flask which was kept at (0-5°C). While maintaining vigorous agitation, 12 g  $\text{KMnO}_4$  was added slowly to the mixture in order to keep the temperature of the suspension below 15°C. The suspension was then transferred to a 35°C bath and vigorously stirred for 2 hrs. After 2 hrs. of stirring, the mixture was heated at 98°C for 10 min. After 10 min, there was a change in temperature to 30 °C which brought about a brown colored solution. Again after 10 min, an additional 200 mL of water was added to dilute the solution. Then, it was followed by a slow addition of the solution and finally treated with 40 mL  $\text{H}_2\text{O}_2$  whereby the color changed to bright yellow. Next, this solution was poured into two separate beakers and stirred for 1 hr. After 1 hr. of stirring, the mixture was washed repeatedly by centrifugation with HCl and deionized water (DI) until it became a gel like substance. After centrifugation, the resulting solid was vacuum dried at 60°C for more than 6 hrs. and became graphene oxide (GO) powder.

##### 4.2 Simultaneous Reduction of Silver and Graphene Oxide

The method for decoration of graphene oxide with silver was reported by Tang et al. (19). First, silver–ammonia solution was prepared by adding an ammonia aqueous solution into a silver nitrate solution ( $\text{AgNO}_3$ ); the concentration of silver nitrate solution was varied, namely 0.1M, 0.2M and 0.3M. Next, it was observed that a brown precipitation appeared until saturation point when it became transparent.

Hereby, synthesized GO powder was added to DI water (0.5mg/ml) and then sonicated for 5 min. PVP solution (4 mg/ml, 1 ml) was firstly mixed with GO suspension (0.5 mg/ml, 10 ml) to form a uniform mixture and glucose (80mg) was then added. Then the mixture was stirred. When the suspension reached 60 degrees Celsius, silver-ammonia solution (1 ml) was added which gave AgNPs/rGO. After reaction, AgNPs/rGO was centrifuged by washing with deionized water (DI) and ethanol, and dried at 80°C.

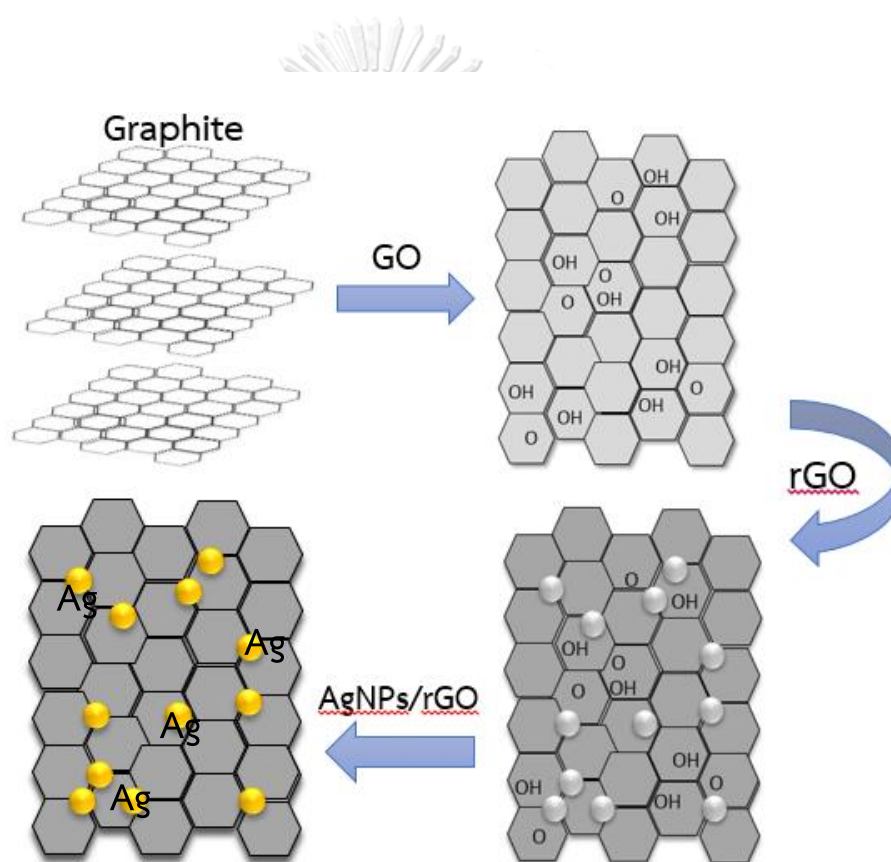


Figure 4 Synthesis of graphene oxide (GO) to silver nanoparticles decorated with reduced graphene oxide (AgNPs/rGO)

### 4.3 Characterization of Products

The presence of silver elements can be identified by energy dispersive x-ray spectroscopy (EDX) and x-ray diffraction pattern (XRD). In Fig.10, the surfaces were observed using field emission scanning electron microscopy (FESEM). The morphology of silver nanoparticles was investigated via transmission electron microscope (TEM). XRD was used to confirm the reduction of graphene oxide (rGO) from graphene oxide (GO). Finally, the samples were examined by a rotating disk electrode (RDE) method for the ORR electrocatalytic properties.

### 4.4 Electrochemical Characterizations

A glassy carbon electrode, 5 mm. in diameter, was rinsed with distilled water and sonicated in acetone. Then, the samples (0.1M, 0.2M and 0.3M) were synthesized and dropped onto a glassy carbon surface. The catalyst films were dried at 30°C for 1 hr. Linear sweep voltammetry (LSV) was performed using a potentiostat system. An electrochemical cell was assembled with a conventional three-electrode system i.e. a glassy carbon working electrode, silver chloride reference electrode and Pt wire counter electrode. The experiments were performed in 0.1M KOH solution:

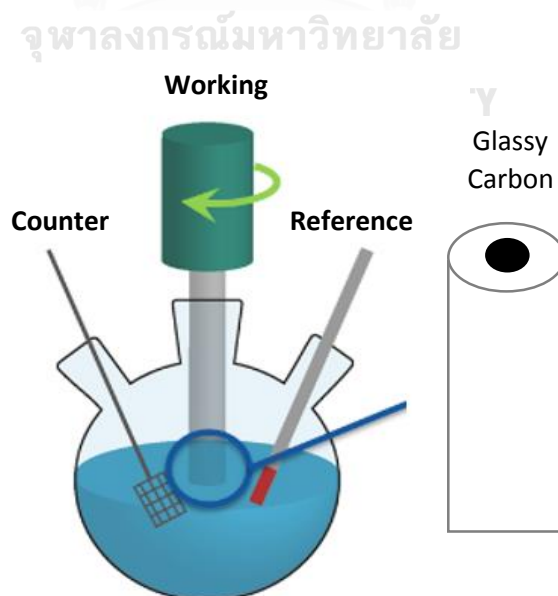


Figure 5 Rotating disk electrode (RDE) and glassy carbon electrode (GC)

## Electrochemical Measurement

- Measurement of linear sweep voltammetry (LSV)

The electrochemical cell was assembled with a conventional three-electrode system: a glassy carbon working electrode, silver chloride reference electrode and platinum wire counter electrode. The experiments were performed in 0.1M KOH solution. Dispersed gas O<sub>2</sub> was saturated for 10 min. The system consisted of: initial potential (0.2) V, end potential (-0.8) V and scan rate (0.05) V/s. The experiment was repeated at 0.1M, 0.2M, and 0.3M (AgNPs/RGO) in 0.1 M KOH solution; a rotating disk electrode (RDE) at several different speeds (400, 900, 1600 rpm) was applied.

From the results of the experiment above, graphs were determined and illustrated as in Fig.11 (A-C). Then, Levich Equation was applied where the diffusion-limited steady current density ( $i_L$ ) is related to the velocity of RDE ( $\omega$  = rpm);  $m$  being the frequency in revolution per minutes, as shown in Eq. 2:

$$i_L = 0.201nFAC_{O_2}D_{O_2}^{2/3}v^{-1/6}\omega^{1/2} \quad (2)$$

However, in the potential range from (0.2-0.8) V, electron-transfer controls the rate of the ORR: the reaction being mixed control. In this region, Koutecky Levich Equation is shown, as in Eq. 3:

$$\frac{1}{i} = \frac{1}{i_k} + \left( \frac{1}{0.201nFC_{O_2}D_{O_2}^{2/3}v^{-1/6}} \right) \omega^{-1/2} \quad (3)$$

where  $i$  is the disk current density,  $i_k$  is the kinetic current density, and  $i_L$  is the Levich current density and where  $n$  ( $mol^{-1}$ ) is the overall electron transfer number.



#### 4.5 Cathode Polarization

Herein, a cathode electrode was prepared using nickel foam which was cut into a circle having a diameter of 5 cm. The cathode electrode consisted of AgNPs / rGO, carbon, PVDF and a solvent DMF. These compositions were mixed together before coating on the nickel foam using a circle 2 cm. in diameter. Finally, all the components were baked until all were dried. Then, the cathode was controlled by the conditions as set out in Table 4. The experiment was assembled for LSV utilizing a potentiostat and a three-electrode system: working electrode, silver chloride electrode as reference electrode and zinc plate as counter electrode. The experiments were performed in 8M KOH solution.

Table 3 The condition of cathode electrodes

Catalyst (%)	Carbon (%)
0.3M AgNPs/rGO 25 %	75 %
0.3M AgNPs/rGO 50 %	50 %
0.3M AgNPs/rGO 75 %	25 %
0.3M AgNPs/rGO 100 %	-

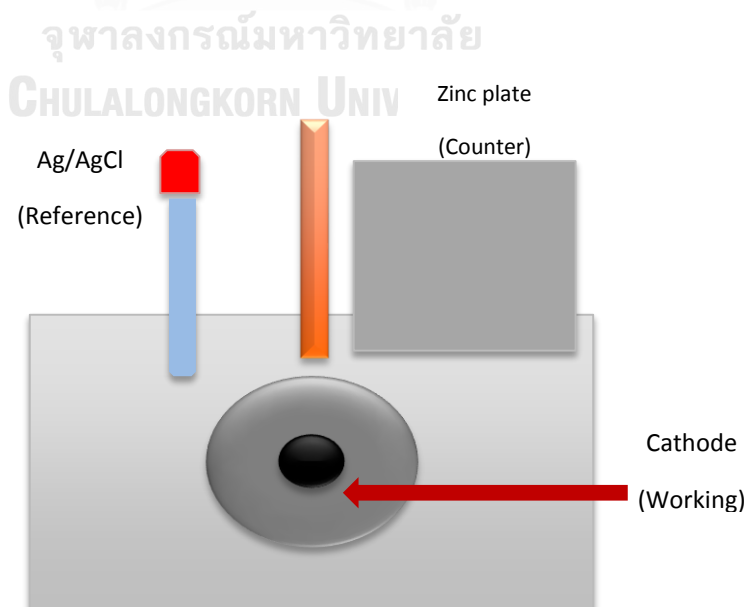


Figure 6 Schematic illustration of cathode polarization experiment

#### 4.6 Battery Cell Design and Fabrication

A zinc air flow battery basically consists of a zinc anode and an air cathode. It is made up of a hollow tube made of stainless steel mesh attached with nipples and a silicone tube. The hollow tube has a diameter of 1 cm and a length of 12 cm. Inside the tube, the anode contains 5g of granular zinc. The anode is wrapped with a PVAc coated filter paper as separator and encased by the cathode. Nickel (Ni) foam coated along with a gas diffusion layer (GDL) and catalyst layer make up the material of the cathode. The gas diffusion layer was composed of 40% carbon, 40% PTFE and 20% glucose which were mixed together and ethanol was used as a dispersion solvent. The catalyst powder, namely (AgNPs / rGO) was dispersed by Dimethylformamide (DMF). Then, the prepared GDL mixture and the catalyst powder were coated on different sides of the cathode. The catalyst side was attached to the separator and the GDL side was in contact with the air. In addition, the active area of the cathode was 4 cm<sup>2</sup>. 9M KOH solution was used as electrolyte. The electrolyte circulated through the cell via a peristaltic pump at 50 RPM.

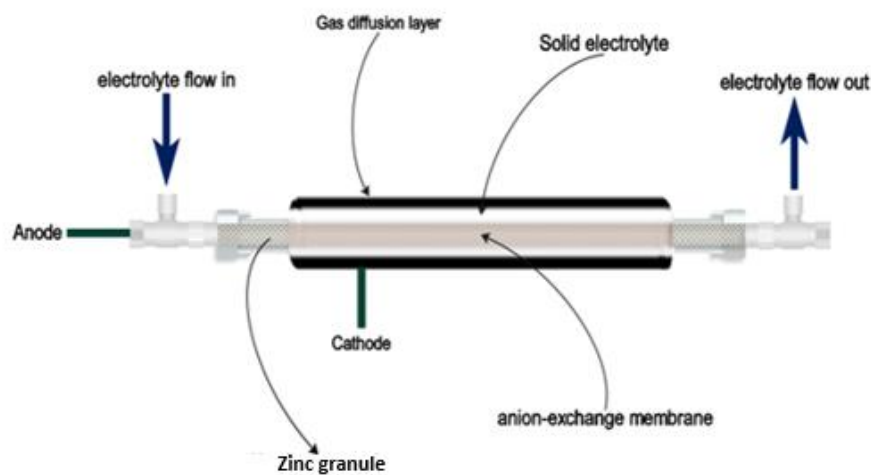


Figure 7 Schematic illustration of Zinc-air cell

## CHAPTER V

### Results and Discussion

#### 5.1 Physiochemical Studies

Silver nanoparticles decorated on graphene sheets were analyzed via transmission electron microscopy (TEM), field emission scanning electron microscopy (FESEM), energy dispersive x-ray spectrometry surfaces (EDX) as well as x-ray diffraction pattern (XRD). The existence of silver nitrate was confirmed by energy dispersive x-ray spectroscopy and x-ray diffraction pattern (XRD):

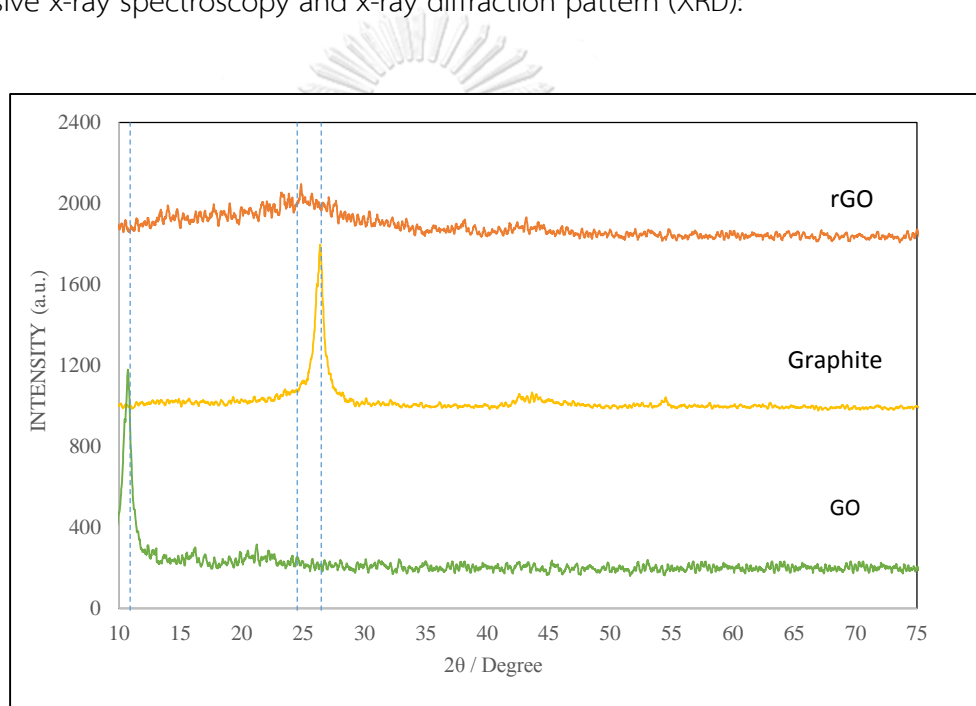


*Figure 8 Powder XRD pattern of reduced graphene oxide (rGO), graphite and graphene oxide (GO)*

The XRD samples were prepared from rGO and AgNPs/rGO powder. The XRD patterns are illustrated in the  $2\theta$  range above between  $5^\circ$  and  $75^\circ$ . According to Fig.8, rGO, graphite and GO exhibited  $2\theta$  peaks at 10.2, 25.2 and 24, respectively. Therefore, the chemical compositions of the samples tested proved to satisfy the theoretical  $2\theta$ , as stated (in Chapter 2 Introduction section 2.2.6.)

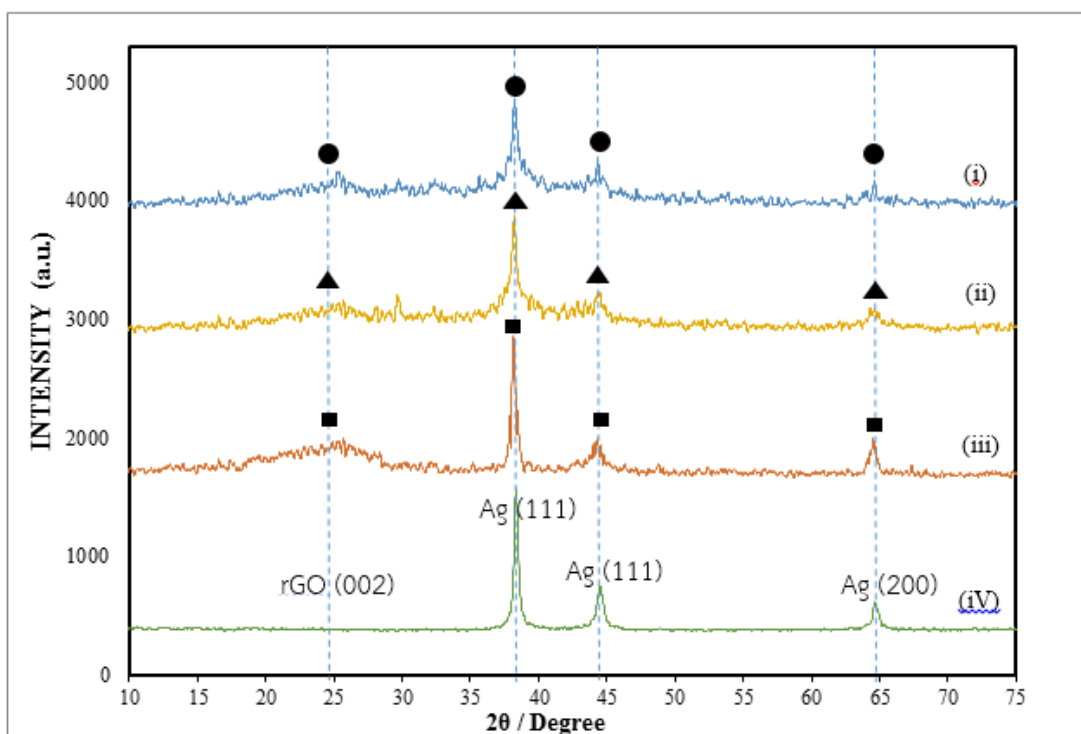


Figure 9 X-ray diffraction patterns of 0.1M AgNPs/rGO (i), 0.2M AgNPs/rGO (ii), 0.3M AgNPs/rGO (iii) and AgNPs (iv)

The silver nitrate samples were displayed on graphene sheets. As shown in Figure 99, the pattern range was examined between  $10^\circ$  and  $75^\circ$  revealing intensity peaks at 24, 38.1, 44.3 and 64.4 degrees for 0.1M, 0.2M and 0.3M concentration, respectively.

In Fig.9, the obtained peaks form a broad reflection at 24.21, corresponding to the (002) plane of rGO. The peaks obtained at 38.1, 44.3 and 64.4 showed strong reflections which are assigned to (111), (200) and (220), respectively. These reflections indicated that the structure of AgNPs was a face-centered cubic structure. According to XRD studies in Fig. 9, the results are consistent because in Fig. 9, the peaks are peaks of silver nanoparticles. Further, peak 24 is the peak of reduced graphene oxide (rGO). This confirms that the chemical composition of the silver nanoparticles decorated on graphene sheets is the catalyst (AgNPs/rGO).

Table 4 Energy dispersive x-ray spectrometry surfaces (EDX) of Ag nanoparticles of AgNPs/rGO that are prepared with different AgNO<sub>3</sub> concentrations.

Catalyst	Energy dispersive x-ray spectrometry surfaces EDX (wt %)	
	Ag	C
0.1M AgNPs/rGO	16.6	75.4
0.2M AgNPs/rGO	18.0	66.8
0.3M AgNPs/rGO	32.5	59.8

Table 4 shows the results of the chemical compositions as calculated via EDX. By controlling the concentration of AgNO<sub>3</sub>, the amount of synthetic substances loaded was determined. In Table 4, the percentages by weight of Silver (Ag) and carbon (C<sub>2</sub>) are shown. The silver content of the AgNPs catalysts on graphene sheets was also determined by EDX. Moreover, the results found that the silver content from EDX corresponded well with the experimental results which are shown in Fig.11.

## 5.2 Particle Size Analysis

In Fig.9, AgNPs/rGO samples were prepared by varying the concentration of AgNO<sub>3</sub> solution i.e. 0.1 M, 0.2M, and 0.3M. The values of the synthesis are shown in the TEM images. According to Fig.15 (a), the image for 0.1M shows that, despite the existence of some larger particles on the graphene sheets, most of the Ag nanoparticles are small. The size ranges of Ag nanoparticles are mostly distributed between 3 and 8 nm, and the mean particle size diameter is 5.76 nm.

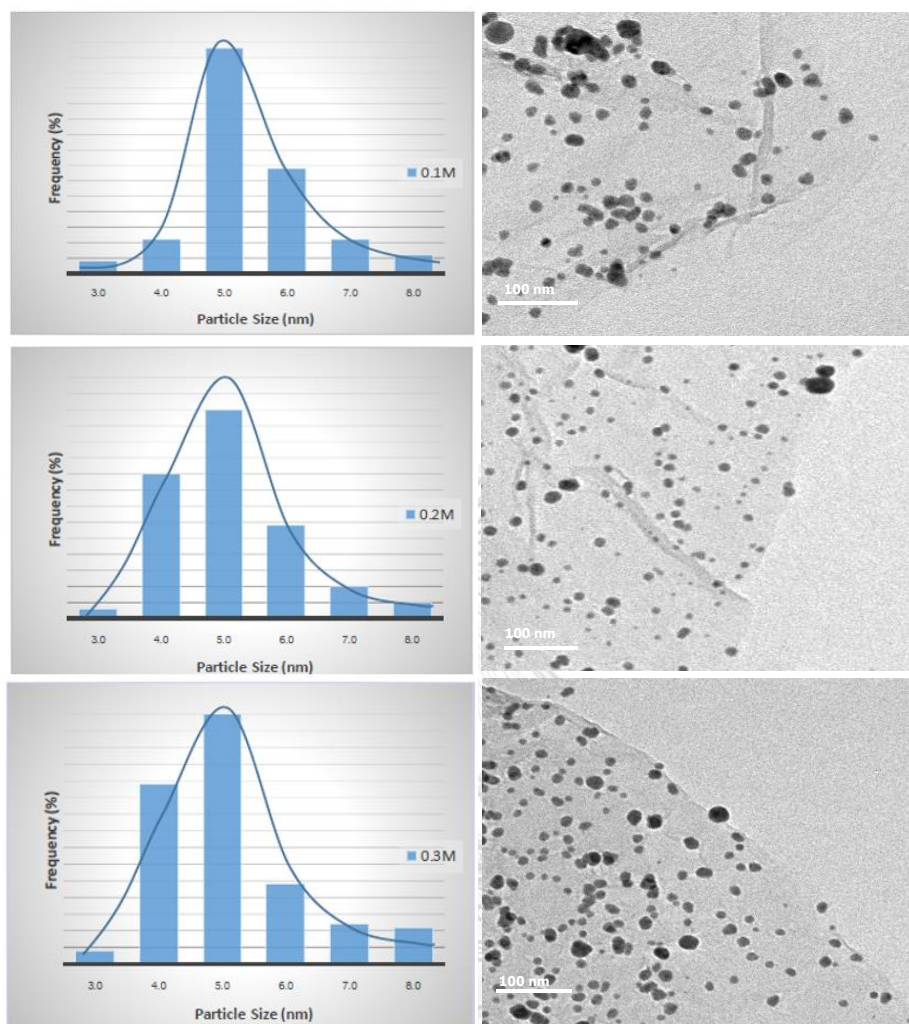


Figure 10 Transmission electron microscopies (TEM) and average size of particles for (a) 0.1M AgNPs/rGO (b) 0.2M AgNPs/rGO and (c) 0.3M AgNPs/rGO

In Fig.11 (b). TEM images of the AgNPs/rGO sample are presented as prepared from 0.2M concentration of  $\text{AgNO}_3$  solution. Thus, it can be seen that the image of 0.2M shows that despite some larger particles, most of the Ag nanoparticles on the graphene sheets are small. The size range of the Ag nanoparticles are mostly distributed between 4 and 8 nm, and the mean particle size diameter is 5.42 nm. In Fig. 9 (c), the image 0.3M reveals that the mean particle size diameter is 5.59 nm. Most of the Ag nanoparticles are small and well dispersed on the graphene sheets. It

is noted that the results above are in agreement with the research, regarding particle size of the silver nanoparticles decorated on graphene sheets, by Kumar et al.(20).

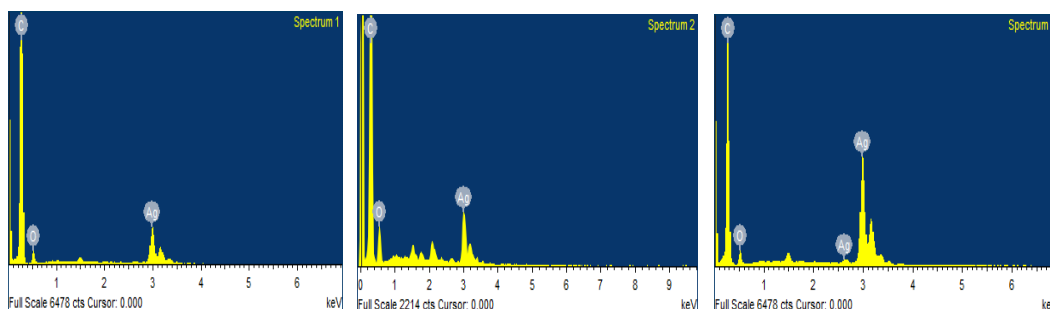


Figure 11 EDX of (a) 0.1M AgNPs/rGO (b) 0.2M AgNPs/rGO and (c) 0.3M AgNPs/rGO

Dispersal of the particles covered a range of approximately 90%, 4–8 nm. The results found that the size of the particles in 0.1M, 0.2M, and 0.3M of AgNO<sub>3</sub> and the distribution of the catalyst at a concentration of 0.1M, 0.2M and 0.3M were the same. Consequently, the size of the particles was not affected by the ORR reaction. As illustrated in Fig.11, the distribution of the catalyst at a concentration of 0.1M, 0.2M and 0.3M showed that the silver nanoparticle dispersion on the graphene sheets was not affected by the ORR reaction.

### 5.3 Electrochemical Studies

In this experiment, linear sweep voltammetry of AgNPs/rGO coated with GC was recorded at a sweep rate of 50 mV s<sup>-1</sup> in 0.1 M KOH solution saturated with O<sub>2</sub> at speeds of RDE (400, 900 and 1600) rpm, as shown in Fig.14 (A-C). The steady-state current due to diffusion controlled the ORR reaction: refer to Equation (1).

A number of electron transfer can be obtained during the potential range from (0.0 to -0.8) V, as the current in this region is not limited by oxygen diffusion. In order to investigate the electron transfer of the 0.1M 0.2M 0.3M (AgNPs/rGO) catalysts toward the ORR, Koutecky–Levich Equation can be applied.

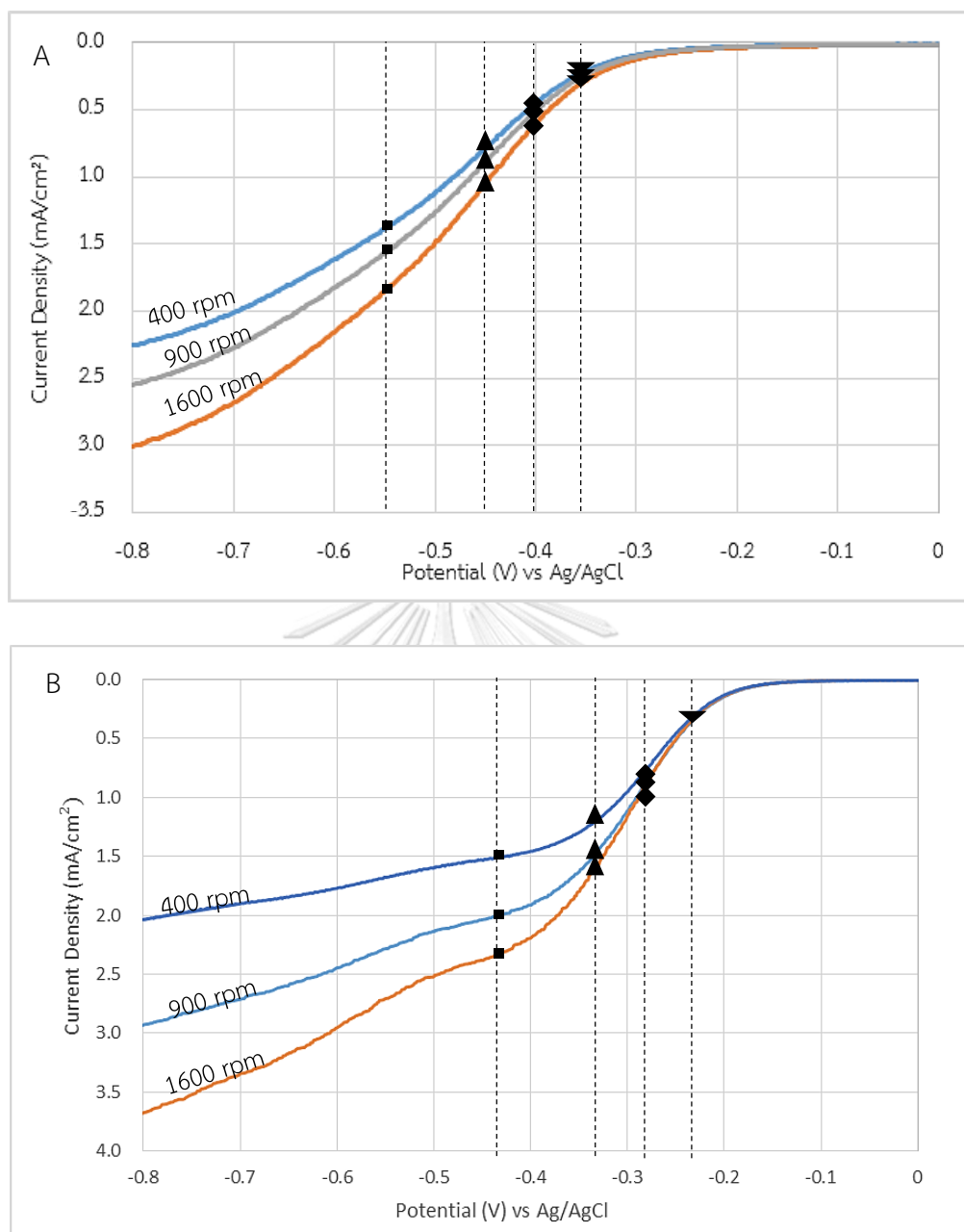


Figure 12 (A-B) Linear sweep voltammety obtained in 0.1 M KOH saturated with O<sub>2</sub> for 0.1 M (AgNPs/rGO), 0.2 M(AgNPs/rGO): scans start at 0.1 V and scan rate 50 mV s<sup>-1</sup>.



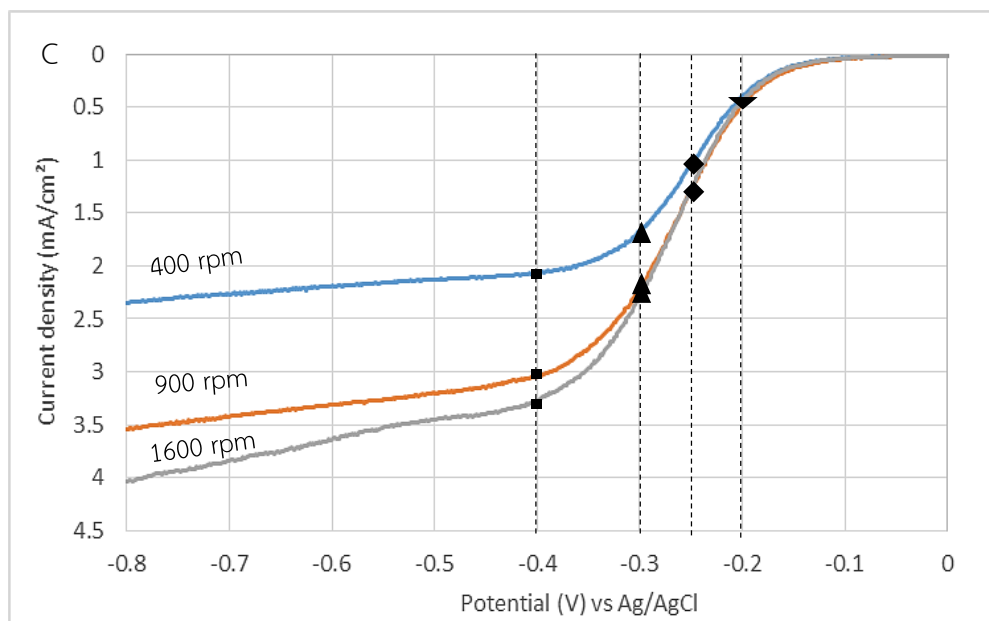


Figure 12 (C) Linear sweep voltammetry obtained in 0.1 M KOH saturated with  $O_2$  for 0.3 M (AgNPs/rGO): scans start at 0.1 V, and scan rate  $50 \text{ mV s}^{-1}$ .

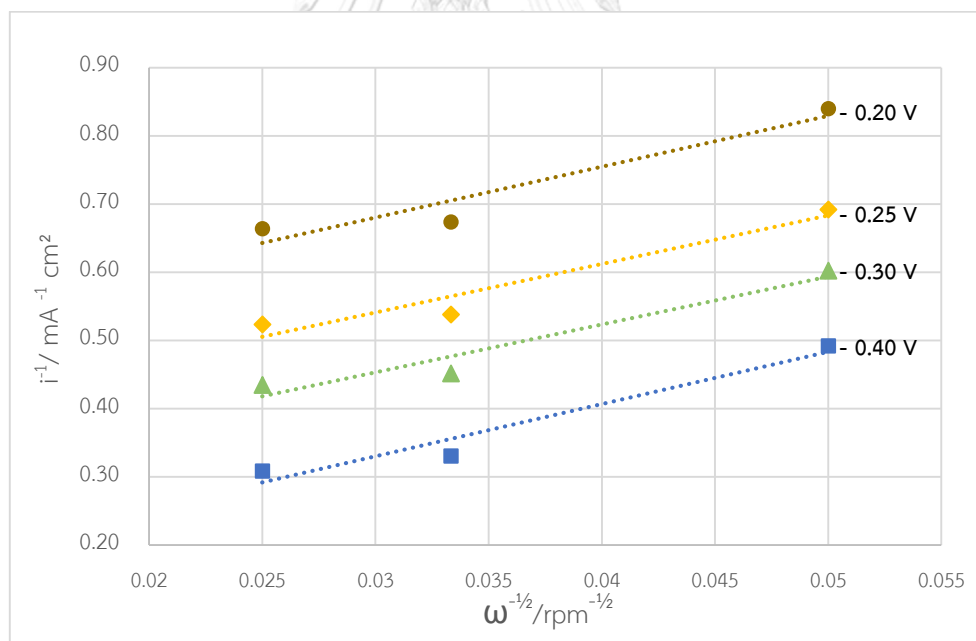


Figure 13 Koutecky–Levich plot. LSV obtained in 0.1 M KOH saturated with  $O_2$  for 0.3M (AgNPs/rGO) at scan rate  $50 \text{ mV s}^{-1}$ .

Linear sweep voltammetry (LSV) was used to record AgNPs/rGO coated with GC at the scan rate of  $50 \text{ mV s}^{-1}$  using different speeds of RDE in 0.1 M KOH solution

saturated with O<sub>2</sub>. During (0.0 to -0.2) V, however, the reduction current, started to increase at -0.2 V. In Fig.12A, the current between (-0.35 to -0.55) V can be said to control both electron transfer and diffusion. The steady-state current, due to diffusion, controlled the ORR reaction. The steady current density ( $i_L$ ) was limited by the diffusion. The velocity of the rotating disk electrode had an effect on the current density; higher rotating speed resulted in faster diffusion.

In Fig. 12B, the current between (-0.24 to -0.44) V can be said to control both electron transfer and diffusion. In Fig.18C, the current between (-0.20 to -0.40) V can also be said to control both electron transfer and diffusion. Again, the velocity of the rotating disk electrode had an effect on current density; higher rotating speed resulted in faster diffusion, in both figures.

In Fig.13 Eq. (3) was employed to calculate and obtain the slope values. Then, the slope values were used to plot graphs of the corresponding  $i^{-1}$  vs.  $\omega^{-1/2}$ . The catalyst samples were tested at various rotating speeds i.e. (400, 900 and 1600) rpm. The corresponding  $i^{-1}$  vs.  $\omega^{-1/2}$  plots, which illustrate linearity at various potentials, fitted the Koutecky-Levich Equation. From the slope of this graph, the number of electron (n) involved in the charge transfer reaction can be calculated, and the intercept of this graph on  $i^{-1}$  axis gives the kinetic current  $i_k$  ( $i_k$  is commonly normalized against the electroactive surface area of the electrode). The diffusion limited is independent of  $i_k$  and the determination of n using the Koutecky-Levich analysis is not affected. (29)

Table 5 the number of electron transfer at varied concentration

E/V (vs Ag/AgCl) AgNPs/rGO	n		
	0.1M	0.2M	0.3M
-0.35	1.24	3.33	3.77
-0.36	1.31	3.30	3.74
-0.37	1.41	3.23	3.65
-0.38	1.53	3.16	3.63
-0.39	1.66	3.09	3.66

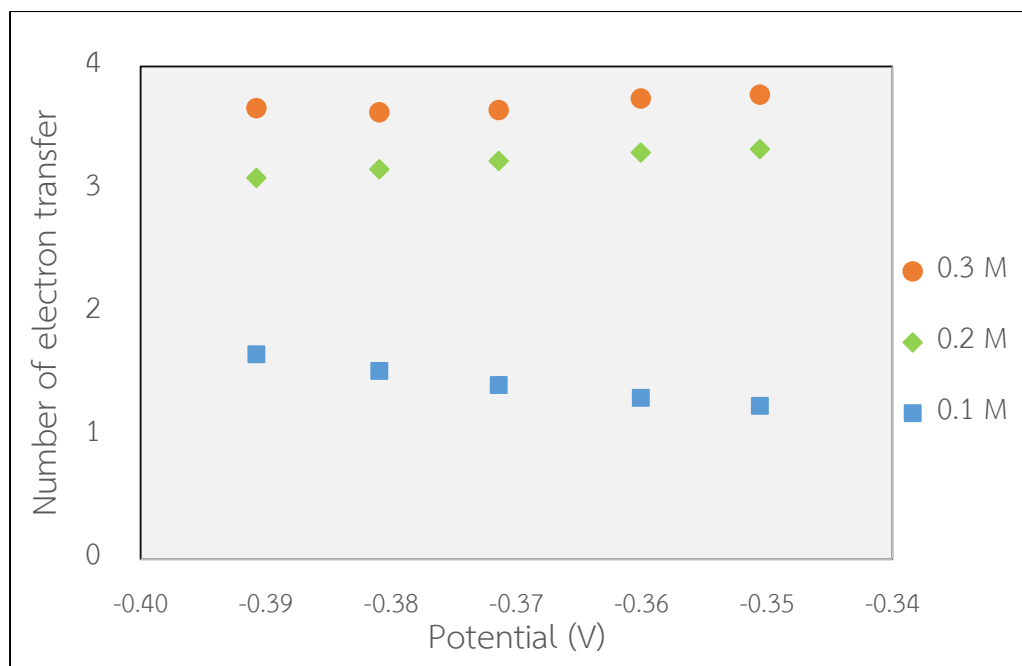


Figure 14 The number of electron transfer (n)

The synthesis of silver nanoparticles decorated on graphene sheets (AgNPs/rGO) was controlled at 0.1M, 0.2M and 0.3M concentration of silver nitrate ( $\text{AgNO}_3$ ). All results are shown in Table 5. Hence, the results, were observed on the average from the potential at (-0.35 to -0.39) V. Therefore, as demonstrated, can be used to determine the number of electron transfer using Koutecky-Levich Equation. At (0.1M, 0.2M and 0.3M) AgNPs / rGO, the number of electron transfer was calculated and the range of 1.2-1.7, 3.0-3.5 and 3.6-3.8 was obtained, respectively.

In previous studies, it was reported that ORR occurs through 4-electron pathway on bulk Ag (30) and 2-electron pathway in the rGO electrode (31). ORR may occur in parallel at the Ag sites which follow 4-electron pathway and may occur at the rGO site which follows 2-electron pathway (28).

According to the three different concentrations i.e. 0.1M 0.2M and 0.3M of AgNPs/rGO, the overall average number of electron transfer is, namely 1.43, 3.22 and 3.69, respectively. Except for the 0.1M AgNPs/rGO, all other AgNPs/rGO catalysts show the ORR via 4-electron pathway. The fact that less than 4 electron transferred on 0.1M AgNPs/rGO is probably due to the low Ag content on the electrode where the

ORR could be catalyzed by carbon via 2-electron pathway (27). The electron transfer was found to be 1.43 which is closer to the 2-electron pathway more than the 4-electron pathway. This is because the mechanism of ORR on 0.1M AgNPs/rGO is more favorable to the 2-electron pathway than the Ag site. Therefore, the low number of electron transferred for ORR on 10 wt % Ag/rGO catalyst observed by Guo et al. is likely because the low Ag loading.

However, the electron transfer at 0.2M and 0.3M AgNPs/rGO favours the 4-electron pathway more than the others because the number of electron transfer is close to 4. The average of  $n$ , from the 0.2M and 0.3M AgNPs/rGO, was found to be 3.22 and 3.69 respectively.

In comparison, the ORR mechanism, regarding 0.2M and 0.3M AgNPs/rGO, was seen to be more favorable to the 4-electron pathway than regards the rGO site. This was because the ORR mechanism contributed to a desirable 4-electron pathway in the 0.2M and 0.3M AgNPs/rGO catalyst. However, the value of 0.3M AgNPs/rGO (3.69) approaches the 4 electron pathway more so than the value of 0.2M AgNPs/rGO (3.22), on account of the increasing amount of Ag. Thus, the value of 0.3M AgNPs/rGO can be seen to reach closer to the 4-electron pathway. Therefore, the catalyst 0.3M AgNPs/rGO can be said to be more favorable to the 4-electron pathway than the other concentration.

*Table 6. A comparison of the number of electron transfer and particle size (nm) of this work with related work in the literature.*

Catalyst	Ag (wt %)	$n$	Particle Size	Literature
Ag/rGO	60%	3.9	10	Lim et al.
Ag/C	60%	2.7	50	Lim et al.
Ag/C	20%	2.3	48	Lima et al.
Ag/C	20%	3.6	15	Demar et al.
AgNPs/rGO	50%	3.9	13	Sun et al.

Catalyst	Ag (wt %)	n	Particle Size	Literature
0.3M AgNPs/rGO	32%	3.69	5.76	This work
0.2M AgNPs/rGO	18%	3.22	5.42	This work
0.1M AgNPs/rGO	15%	1.43	5.59	This work

Table 6. Lim et al.(21) reported that the loading (60%) of high Ag and good distribution results in good ORR reaction. Hereby, the electron transfer reached 4 which corresponded to the result obtained in this thesis. By increasing the amount of silver, the number of electron transfer was closer to 4. Although the silver loading (32%) in this thesis was less than Lim et al. reported, the result is not much different; the electron transfer being close to Lim et al. Therefore, it should be noted that loading of this quantity of silver was sufficient to produce a direct 4-electron pathway.

The electrocatalytic activities of the 0.1M, 0.2M and 0.3M AgNPs/rGO were studied using the RDE technique. The ORR activities, after saturation with O<sub>2</sub> gas in 0.1M KOH solution, were investigated using linear sweep voltammetry (LSV) having a sweep rate of 50 mV s<sup>-1</sup>. In Fig.15, typical LSV curves for 0.1 M, 0.2 M and 0.3 M AgNPs/rGO together with a glassy carbon catalyst at 1600 rpm are shown. The current density at 1600 rpm was chosen for plotting. This was because at 1600 rpm it had the highest current density as compared to (400 and 900) rpm in different concentration, as shown in Table 7.

Table 7 Results of current density at varied concentration of (AgNPs/rGO)

Concentration (AgNPs/rGO)	Current Density (mA/cm <sup>2</sup> )		
	400 rpm	900 rpm	1600 rpm
0.1 M	2.24	2.59	2.99
0.2 M	2.03	2.91	3.66
0.3 M	2.35	3.51	4.02

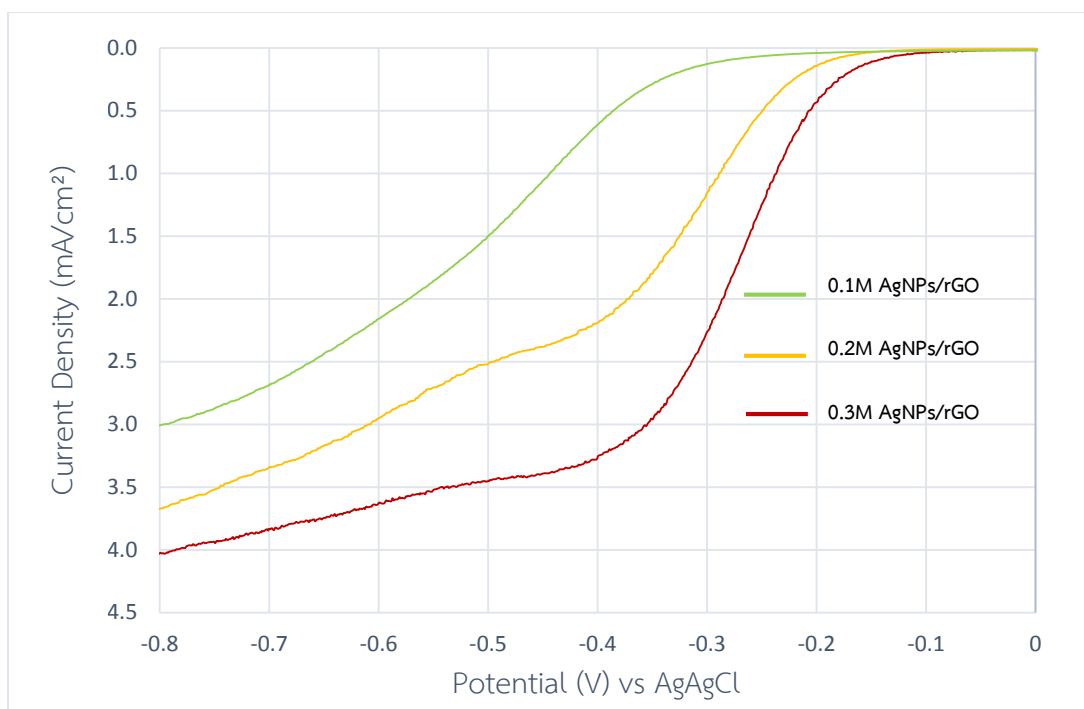


Figure 15 Linear sweep voltammetry rotating disk electrode (RDE) curves of commercial 0.1M AgNPs/rGO , 0.2M AgNPs/rGO and 0.3M AgNPs/rGO in O<sub>2</sub>-saturated 0.1 M KOH with a scan rate of 50 mV s<sup>-1</sup> at 1600 rpm

As illustrated in Fig.15, ORR onset potential of 0.3 M AgNPs/rGO is at -0.13 V which is the highest when compared to the ORR onset potential of 0.2 M AgNPs/rGO, and 0.1M AgNPs/rGO, -0.20V, -0.30V respectively. Thus, the ORR onset potential shifts positively with Ag loading increasing from 0.3M, 0.2M and 0.1M (AgNPs/rGO) respectively. Furthermore, the ORR current density at -0.8 V vs Ag/AgCl is shown in this figure. The current density of 0.3M AgNPs/rGO is 4.02 mA/cm<sup>2</sup> and is much higher than other concentrations. The current density of 0.2M AgNPs/rGO and 0.1M AgNPs/rGO is, namely 3.66 mA/cm<sup>2</sup> and 2.99 mA/cm<sup>2</sup> respectively. Consequently, these results show that the ORR activity of 0.3M AgNPs/rGO is better than 0.1M and 0.2M AgNPs/rGO. As a result of the rotating disk electrode analysis (RDE), the higher concentration of AgNPs provided onset potential shifts positively, higher current density and the number of electron transfer approached 4.

It can be concluded that the ORR reaction produced by the catalyst and synthesized from controlling the three silver concentrations depended on the following: (1) the concentration of silver loading (2) size of silver nanoparticles on graphene sheets (3) the reaction mechanisms on graphene sheets. However, it is noted that the particle size of catalysts in the three concentrations are very similar. Therefore, size does not affect ORR reaction. Thus, catalysts should emphasize that the effectiveness of the ORR can be enhanced by increasing the Ag loading through optimization of the ORR reaction.

To conclude, the catalyst at 0.3M can be seen to be the most effective. It has a higher value than the others, being closer to 4 than the others. Therefore, it is evident that the catalyst at 0.3M (AgNPs/rGO) is the most suitable catalyst on the cathode electrode in the zinc air battery.

#### 5.4 Cathode Polarization

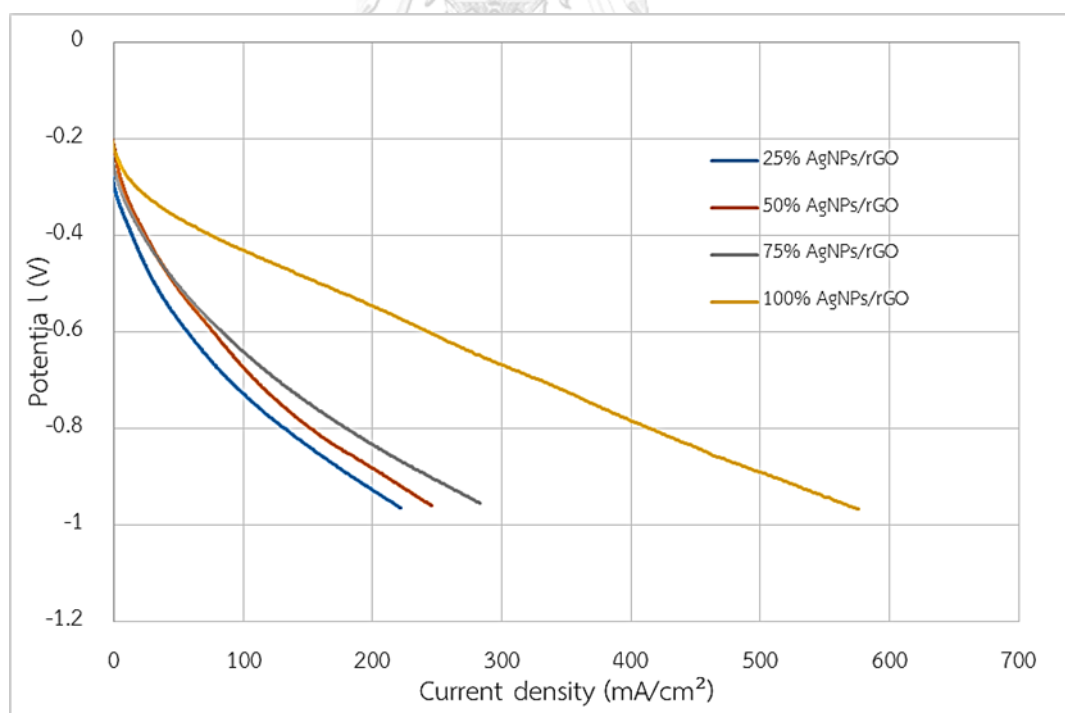


Figure 16 Cathode polarization curve.

As regards cathode polarization efficiency, this test operated under experimental conditions and the data are shown in the LSV graph (Fig.16). When the

current was measured under various conditions, the highest current was obtained using 100% catalysts (AgNPs/rGO). On the other hand, when the catalysts were used with carbon additives, they gave a lower current as compared to the pure catalyst (AgNPs/rGO). When the current increased, the percentage of the catalyst increased. The reason for this is that the pure catalyst can conduct electricity by itself.

## 5.5 Battery Analysis

The batteries were analyzed by a zinc air battery analyzer for polarization curves and discharge curves.

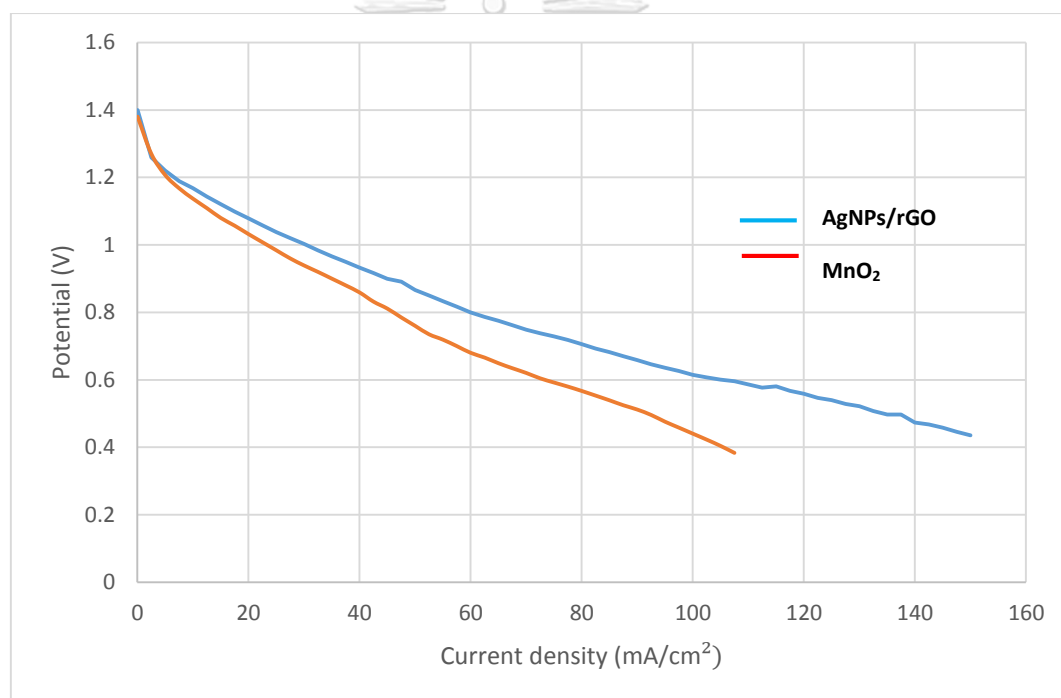


Figure 17 Comparison of discharge polarization curves for performance of zinc air batteries with AgNPs/rGO and MnO<sub>2</sub> catalyst in air.

In Fig.17, discharge polarization curves are shown for the performance of zinc air batteries with AgNPs/rGO and MnO<sub>2</sub> catalyst in air. The developed electrocatalysts were characterized and evaluated in a designed zinc air battery. The battery has a zinc electrode with an excess capacity which makes the performance of the battery depend on the air electrode. The results as plotted reveal that the zinc air battery



with the AgNPs/rGO air electrode is seen to have a much better performance than the battery with the MnO<sub>2</sub> air electrode. The open-circuit voltages of 0.3M AgNPs/rGO and MnO<sub>2</sub> batteries are 1.4V and 1.38V, respectively. When the current increased, the potential of both batteries slowly dropped due to ohmic loss.

In the beginning, the AgNPs/rGO potential dropped lower than the MnO<sub>2</sub> potential since it followed the cathodic polarization in the previous section. The potential of MnO<sub>2</sub> dropped to 0.388 V and 107.5 mA/cm<sup>2</sup>. The potential of AgNPs/rGO dropped to 0.435V and 150 mA/cm<sup>2</sup>. Probably, the higher current density value of AgNPs/rGO was due to higher electron transfer in ORR activity.

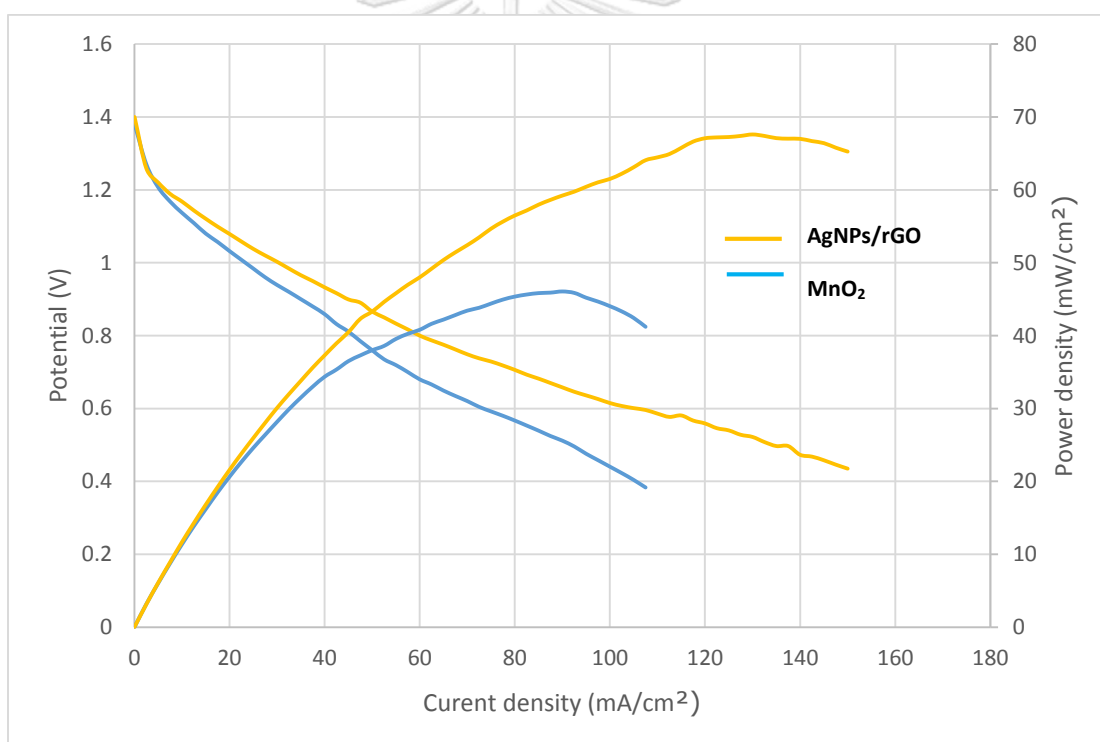


Figure 18 Comparison of power density plots of discharge curves for performance of zinc air batteries with AgNPs/rGO and MnO<sub>2</sub> catalyst in air.

Fig.18 shows comparison of polarization curve of a zinc air battery with 0.3M AgNPs/rGO and MnO<sub>2</sub>. According to the electrical measurements in the zinc air battery, the maximum current density was 150 and 130 mA/cm<sup>2</sup> respectively. Peak

power density of AgNPs/rGO was 67.6 mW/cm<sup>2</sup> at a current density of 130 mA/cm<sup>2</sup>. Peak power density of MnO<sub>2</sub> was 46 mW/cm<sup>2</sup> at a current density of 87.5 mA/cm<sup>2</sup>.

Table.8 below shows that the battery using synthesized catalysts (AgNPs/rGO) gives a higher battery performance. However, results may differ depending on different conditions in the experiment.

In Fig.18, polarization discharge curves are presented. According to the figures, when voltages descend to 1 V, the current densities of the batteries with the AgNPs/rGO and MnO<sub>2</sub> catalysts are 32.5 and 27.5 mA/cm<sup>2</sup>, respectively. In addition, peak power density of the zinc air battery with AgNPs/rGO and MnO<sub>2</sub> reaches 67.6 mW/cm<sup>2</sup> and 46 mW/cm<sup>2</sup>. Thus, power density of the zinc air battery with the AgNPs/rGO catalyst is higher than the MnO<sub>2</sub> catalyst, which confirms the results from the cathodic polarization. In conclusion, it is noted that the zinc air battery that uses the synthesized catalysts (AgNPs/rGO) is a cathode catalyst and gives a better performance than when MnO<sub>2</sub> is used as a catalyst.

Table 8 A comparison of zinc-air battery performance in this work with related work in the literature.

Air cathode	Anode/electrolyte	Potential/Current density @ peak power density (V/mA cm <sup>-2</sup> )	Peak Power density (mW cm <sup>-2</sup> )	References
AgNPs/rGO	Zn granular/9 M KOH	0.522/150	67.6	This work
MnO <sub>2</sub>	Zn granular/9 M KOH	0.511/107.5	46	This work
MnO <sub>2</sub> loaded on Carbon Paper	Zn sheet/6 M KOH	0.5/30	19.5	(32)
MnO <sub>2</sub> power	Zn plate/6 M KOH	-/100	48	(33)
MnO <sub>2</sub> /XC72	Zn plate/6 M KOH Zn plate/6 M KOH + 0.4	0.7/105.25	67.51	(34)
a-MnO <sub>2</sub> -LaNiO <sub>3</sub> /CNT	6 M ZnO	0.6/81	55.1	(35)

## CHAPTER VI

### CONCLUSIONS

#### 6.1 Conclusions

This thesis focused on the development of a cathode for a zinc air battery. First, the research proceeded by the synthesis of graphene oxide (GO) using the Hummer method. Next, silver nanoparticles decorated on reduced graphene oxide (AgNPs/rGO) at varied concentration, namely 0.1M, 0.2M and 0.3M were synthesized using glucose reduction method. All catalysts were studied in terms. The structure and morphology of AgNPs/rGO was checked using X-ray diffraction (XRD). Further, transmission electron microscopy (TEM) analyzes were carried out. The amount of Ag contained in each concentration was confirmed via energy dispersive x-ray spectroscopy (EDX). The synthetic catalyst at 3 concentration, using rotating disk electrode (RDE), led to the finding of the transfer of electrons. When the electron transfer was found by means of the catalyst at different concentration, it was observed that by increasing the concentration of Ag in the catalyst the electron transfer rate became closer to 4. Thus, it was found that by increasing the concentration of Ag, the performance of the catalyst increased as well. Consequently, the results showed that 0.3 M concentration gave the highest value of 4 electron pathway and the highest catalyst performance. Based on cathodic polarization measurements, it is possible to conclude that the condition at 100% AgNPs / rGO without carbon had the greatest potential. On the other hand, when carbon was added, it was likely to decrease the current density. The zinc air battery was assembled using 100% (0.3M AgNPs/rGO) condition on the cathode side. Hence, the catalyst 100% (0.3M AgNPs/rGO) gave higher performance than the MnO<sub>2</sub> catalyst. The synthesized catalyst reached a current density and a power density of 150 mA / cm<sup>2</sup> at 0.435 v and 67.6mW / cm<sup>2</sup> at 130 mA / cm<sup>2</sup>, respectively.

## 6.2 Recommendations and Further Studies

This research focused on the development of a cathode for a zinc air battery. The research also focused on increasing the performance of the zinc air battery. It was found that the catalyst 100% AgNPs/rGO used at 0.3M concentration proved to enhance battery performance, providing extra power, thereby increasing its efficiency.

In the long term, further studies on the cathode and electrolyte can lead to optimized battery performance, ensuring its durability and increased time span. Zinc air batteries hold the greatest promise for future energy applications because of their high energy densities and low cost.



## REFERENCES



จุฬาลงกรณ์มหาวิทยาลัย  
**CHULALONGKORN UNIVERSITY**

## APPENDIX A

### CALCULATION NUMBER OF ELECTRON TRANSFER

When the potential is selected from the region where the current is under a mixture of kinetic and mass transfer control, the Koutecky-Levich plot is linear according to equation.

$$\frac{1}{i} = \frac{1}{i_k} + \left( \frac{1}{0.201nFC_{O_2}D_{O_2}^{2/3}\nu^{-1/6}} \right) \omega^{-1/2} \quad (A.1)$$

For equations, the variables is defined as: The Levich and the Koutecky-Levich plots can be fitted using linear regression to calculate the slopes and intercepts. For the Koutecký-Levich plot.

Parameter	Value	Unit
F Faraday's constant	96485	C/mol
A the geometric area of the disk	0.2	cm <sup>2</sup>
C <sub>O<sub>2</sub></sub> the concentration of O <sub>2</sub> in the electrolyte	1.21E-06	mol cm <sup>-3</sup>
*D <sub>O<sub>2</sub></sub> <sup>2/3</sup> the diffusion coefficient of O <sub>2</sub> in the electrolyte	7.12E-04	cm <sup>2</sup> s <sup>-1</sup>
** ν <sup>-1/6</sup> the kinematic viscosity of the electrolyte	2.1544	cm <sup>2</sup> s <sup>-1</sup>
ω the angular frequency of rotation	400, 900, 1600	rpm
n the number of electrons involved in the reaction	This work	-

\* D<sub>O<sub>2</sub></sub>= 1.9E-05, \*\* ν =0.010

The Koutecký-Levich plot is used to calculate the number of electrons. Which analyzed by the catalyst at different concentration (0.1, 0.2M, 0.3M). Then, plot graph between frequency of rotation (x-axis) and current density (y-axis). The slope of 0.1M, 0.2M, and 0.3M (AgNPs/rGO) are shown in Fig A.1, A.2 and A.3, respectively.

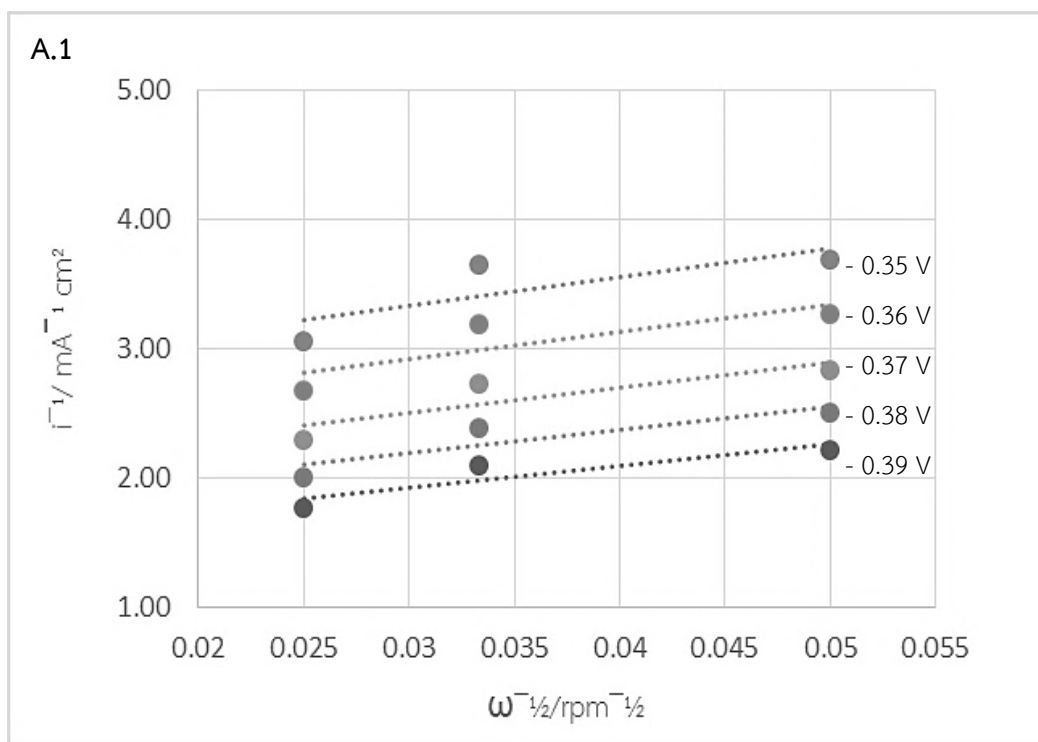


Figure A.1 Koutecky–Levich plot for 0.1M, 0.2M and 0.3M (AgNPs/rGO)

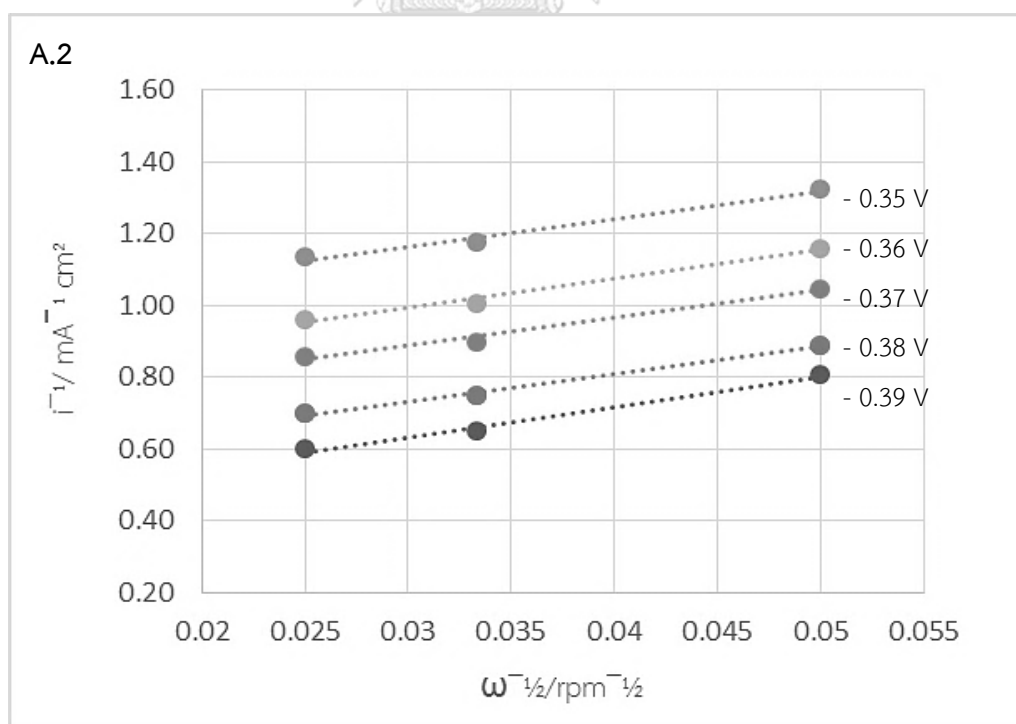


Figure A.2 Koutecky–Levich plot for 0.1M, 0.2M and 0.3M (AgNPs/rGO)

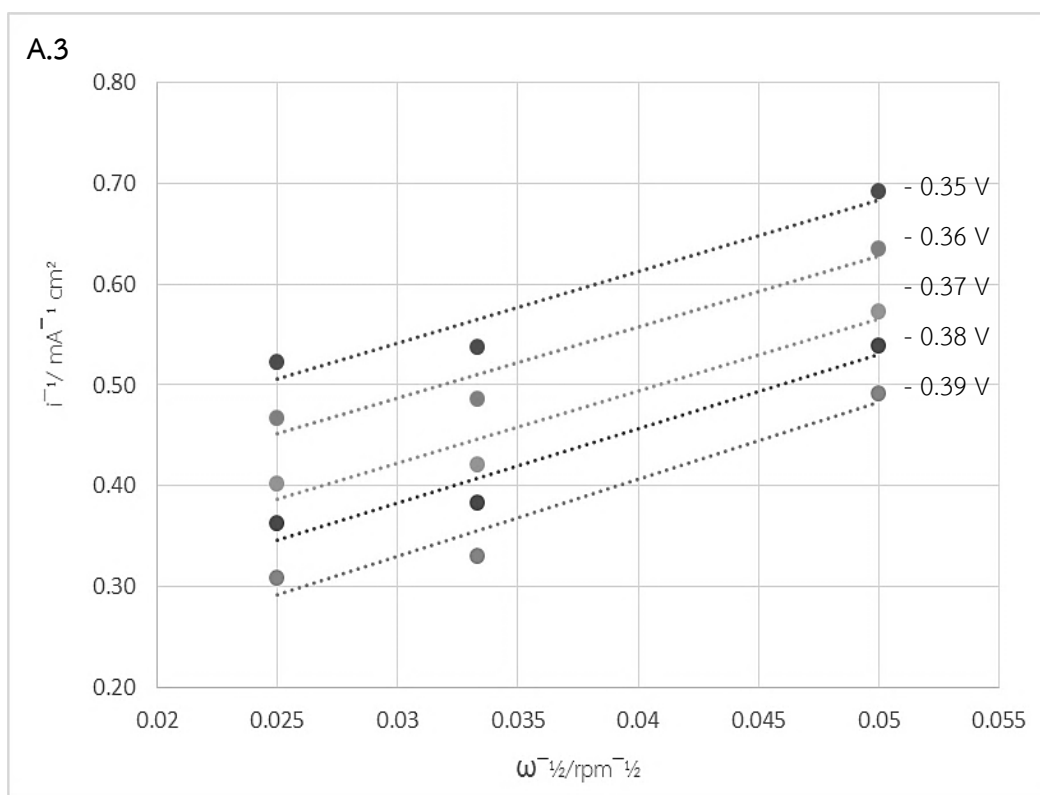


Figure A.3 Koutecky-Levich plot for 0.1M, 0.2M and 0.3M (AgNPs/rGO)

Table A.1 The slope from Koutecky-Levich plot (A.1, A.2 and A3)

Potential (V)/ $\omega$	400 rpm	900 rpm	1600 rpm
-0.35	3.697388	3.656855	3.0554723
-0.36	3.27149	3.192397	2.6721666
-0.37	2.84005	2.734381	2.2928315
-0.38	2.50934	2.391497	2.0079723
-0.39	2.219464	2.096614	1.762387
-0.35	1.322482	1.177397	1.1338321
-0.36	1.157961	1.007393	0.9612395
-0.37	1.04641	0.897972	0.8577552
-0.38	0.890113	0.746918	0.7012618



-0.39	0.805399	0.649078	0.5988405
-0.35	0.691985	0.538061	0.5232859
-0.36	0.636035	0.486834	0.4670347
-0.37	0.573761	0.421294	0.4028491
-0.38	0.539016	0.383621	0.3626357
-0.39	0.491811	0.330703	0.3087261

Table A.2 The number of electron transfer 0.1M, 0.2M and 0.3M (AgNPs/rGO)

Potential(V)	0.1 M AgNPs/rGO	0.2 M AgNPs/rGO	0.3 M AgNPs/rGO
-0.35	1.24	3.33	3.77
-0.36	1.31	3.30	3.74
-0.37	1.41	3.23	3.65
-0.38	1.53	3.16	3.63
-0.39	1.66	3.09	3.66
Average	1.43	3.43	3.69

## EXPERIMENTAL DATA

In following, more details of experimental data for this thesis are given.

- B1. Zinc air battery with AgNPs/rGO catalyst in cathode side

The following Zinc air battery experimental data were plotted as polarization curve which was used to compare with simulation result in section 5.5 (Fig.19).

- B2. Zinc air battery with MnO<sub>2</sub> catalyst in cathode side

The following Zinc air battery experimental data were plotted as polarization curve which was used to compare with simulation result in section 5.5 (Fig.19).

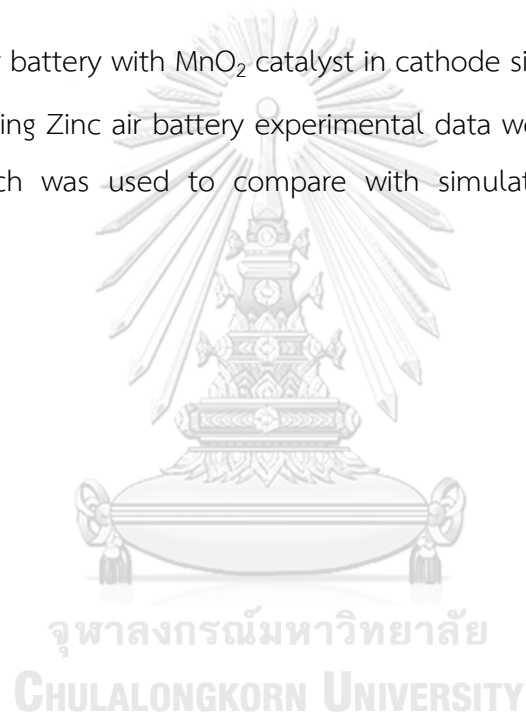


Table B.1 Experimental performance data for Zinc air battery with AgNPs/rGO catalyst in cathode side

Current Density (mA/cm <sup>2</sup> )	Voltage (V)	Power Density (mW/cm <sup>2</sup> )	Current Density (mA/cm <sup>2</sup> )	Voltage (V)	Power Density (mW/cm <sup>2</sup> )	Current Density (mA/cm <sup>2</sup> )	Voltage (V)	Power Density (mW/cm <sup>2</sup> )	Current Density (mA/cm <sup>2</sup> )	Voltage (V)	Power Density (mW/cm <sup>2</sup> )
0.0	1.400	0.000	42.5	0.917	38.951	85.0	0.682	57.970			
2.5	1.259	3.148	45.0	0.899	40.469	87.5	0.670	58.625			
5.0	1.220	6.100	47.5	0.891	42.299	90.0	0.658	59.220			
7.5	1.189	8.918	50.0	0.866	43.303	92.5	0.646	59.755			
10.0	1.168	11.680	52.5	0.850	44.625	95.0	0.636	60.420			
12.5	1.143	14.293	55.0	0.833	45.815	97.5	0.626	61.035			
15.0	1.121	16.811	57.5	0.817	46.978	100.0	0.615	61.500			
17.5	1.099	19.233	60.0	0.800	48.000	102.5	0.607	62.218			
20.0	1.079	21.580	62.5	0.787	49.188	105.0	0.601	63.105			
22.5	1.058	23.810	65.0	0.775	50.375	107.5	0.596	64.070			
25.0	1.038	25.950	67.5	0.762	51.435	110.0	0.586	64.460			
27.5	1.020	28.047	70.0	0.749	52.416	112.5	0.577	64.913			
30.0	1.003	30.081	72.5	0.738	53.483	115.0	0.581	65.760			
32.5	0.984	31.980	75.0	0.729	54.675	117.5	0.567	66.623			
35.0	0.966	33.803	77.5	0.718	55.645	120.0	0.559	67.080			
37.5	0.950	35.616	80.0	0.706	56.480	122.5	0.546	67.200			
40.0	0.933	37.300	82.5	0.693	57.173	125.0	0.540	67.250			

Table B.2 Experimental performance data for Zinc air battery with MnO<sub>2</sub> catalyst in cathode side

Current (mA/cm <sup>2</sup> )	Voltage (V)	Power Density (mW/cm <sup>2</sup> )	Current (mA/cm <sup>2</sup> )	Voltage (V)	Power Density (mW/cm <sup>2</sup> )	Current (mA/cm <sup>2</sup> )	Voltage (V)	Power Density (mW/cm <sup>2</sup> )	Current (mA/cm <sup>2</sup> )	Voltage (V)	Power Density (mW/cm <sup>2</sup> )
0.0	1.380	0.048	42.5	0.832	35.350	85.0	0.539	45.835			
2.5	1.270	3.175	45.0	0.811	36.500	87.5	0.525	45.900			
5.0	1.207	6.035	47.5	0.785	37.288	90.0	0.512	46.060			
7.5	1.168	8.760	50.0	0.760	38.000	92.5	0.496	45.863			
10.0	1.137	11.370	52.5	0.735	38.588	95.0	0.476	45.205			
12.5	1.109	13.863	55.0	0.719	39.550	97.5	0.458	44.675			
15.0	1.080	16.200	57.5	0.700	40.250	100.0	0.440	44.040			
17.5	1.057	18.498	60.0	0.680	40.800	102.5	0.423	43.325			
20.0	1.032	20.640	62.5	0.666	41.625	105.0	0.404	42.425			
22.5	1.008	22.680	65.0	0.649	42.200	107.5	0.383	41.210			
25.0	0.984	24.600	67.5	0.634	42.825						
27.5	0.960	26.400	70.0	0.620	43.430						
30.0	0.939	28.170	72.5	0.604	43.825						
32.5	0.920	29.900	75.0	0.592	44.400						
35.0	0.900	31.500	77.5	0.580	44.950						
37.5	0.880	33.000	80.0	0.567	45.360						
40.0	0.859	34.360	82.5	0.553	45.640						

### VITA

Miss Laksanaporn Poolnapol was born in Chonburi, Thailand on July 8, 1992. She graduated from Chonkanyanukoon High School, Chonburi in 2010. She started her Bachelor's Degree in Chemical Engineering from King Mongkut's Institute of Technology, Ladkrabang in 2011. She finished her Bachelor's Degree in 2015. After this, she continued her studies in 2016 at Chulalongkorn University where she enrolled on the Master's Degree Program in Chemical Engineering.



1. Kheawhom S, Suren S. Printed air cathode for flexible and high energy density zinc-air battery 2016. 1-7 p.
2. Zhang J. PEM Fuel Cell Electrocatalysts and Catalyst Layers: Fundamentals and Applications 2008.
3. Suren S, Kheawhom S. Development of a High Energy Density Flexible Zinc-Air Battery 2016. A846-A50 p.
4. Caramia V, Bozzini B. Materials science aspects of zinc-air batteries: a review. *Materials for Renewable and Sustainable Energy*. 2014;3(2):28.
5. Råde I, Andersson BA. Requirement for metals of electric vehicle batteries. *Journal of Power Sources*. 2001;93(1):55-71.
6. Zhu S, Chen Z, Li B, Higgins D, Wang H, Li H, et al. Nitrogen-doped carbon nanotubes as air cathode catalysts in zinc-air battery. *Electrochimica Acta*. 2011;56(14):5080-4.
7. Song C, Zhang J. Electrocatalytic Oxygen Reduction Reaction. In: Zhang J, editor. *PEM Fuel Cell Electrocatalysts and Catalyst Layers: Fundamentals and Applications*. London: Springer London; 2008. p. 89-134.
8. Lee J-S, Tai Kim S, Cao R, Choi N-S, Liu M, Lee KT, et al. Metal-Air Batteries with High Energy Density: Li-Air versus Zn-Air. *Advanced Energy Materials*. 2011;1(1):34-50.
9. Wang F-B, Wang J, Shao L, Zhao Y, Xia X-H. Hybrids of gold nanoparticles highly dispersed on graphene for the oxygen reduction reaction. *Electrochemistry Communications*. 2014;38:82-5.
10. Jiang L, Hsu A, Chu D, Chen R. Oxygen reduction reaction on carbon supported Pt and Pd in alkaline solutions. *Journal of the Electrochemical Society*. 2009;156(3):B370-B6.
11. Spendelow JS, Wieckowski A. Electrocatalysis of oxygen reduction and small alcohol oxidation in alkaline media. *Physical Chemistry Chemical Physics*. 2007;9(21):2654-75.
12. Shih CJ, Vijayaraghavan A, Krishnan R, Sharma R, Han JH, Ham MH, et al. Bi- and Trilayer Graphene Solutions. *Nat Nanotechnol*. 2011;6:439.

13. Zhanga J, Zhaoa XS. Graphene-Based Materials for Electrochemical Energy Storage. Two-Dimensional Carbon: Fundamental Properties, Synthesis, Characterization, and Applications. 2014:183.
14. Lopes JH, Ye S, Gostick JT, Barralet JE, Merle G. Electrocatalytic Oxygen Reduction Performance of Silver Nanoparticle Decorated Electrochemically Exfoliated Graphene. *Langmuir*. 2015;31(35):9718-27.
15. Li Y, Dai H. Recent advances in zinc-air batteries. *Chemical Society Reviews*. 2014;43(15):5257-75.
16. Li Y, Dai H. Recent advances in zinc-air batteries. *Chemical Society Reviews*. 2014;43(15):5257-75.
17. Song C, Zhang J. Electrocatalytic oxygen reduction reaction. PEM fuel cell electrocatalysts and catalyst layers: Springer; 2008. p. 89-134.
18. Treimer S, Tang A, Johnson DC. A Consideration of the application of Koutecký-Levich plots in the diagnoses of charge-transfer mechanisms at rotated disk electrodes. *Electroanalysis*. 2002;14(3):165-71.
19. Tang X-Z, Li X, Cao Z, Yang J, Wang H, Pu X, et al. Synthesis of graphene decorated with silver nanoparticles by simultaneous reduction of graphene oxide and silver ions with glucose. *Carbon*. 2013;59:93-9.
20. Kumar S, Selvaraj C, G Scanlon L, Munichandraiah N. Ag nanoparticles-anchored reduced graphene oxide catalyst for oxygen electrode reaction in aqueous electrolytes and also a non-aqueous electrolyte for Li-O<sub>2</sub> cells 2014.
21. Lim EJ, Choi SM, Seo MH, Kim Y, Lee S, Kim WB. Highly dispersed Ag nanoparticles on nanosheets of reduced graphene oxide for oxygen reduction reaction in alkaline media. *Electrochemistry Communications*. 2013;28:100-3.
22. Soo LT, Loh KS, Mohamad AB, Daud WRW, Wong WY. Synthesis of silver/nitrogen-doped reduced graphene oxide through a one-step thermal solid-state reaction for oxygen reduction in an alkaline medium. *Journal of Power Sources*. 2016;324:412-20.
23. Xu M, Ivey DG, Xie Z, Qu W. Rechargeable Zn-air batteries: Progress in electrolyte development and cell configuration advancement. *Journal of Power Sources*. 2015;283(Supplement C):358-71.

24. Wang T, Kaempgen M, Nopphawan P, Wee G, Mhaisalkar S, Srinivasan M. Silver nanoparticle-decorated carbon nanotubes as bifunctional gas-diffusion electrodes for zinc–air batteries. *Journal of Power Sources*. 2010;195(13):4350-5.
25. Cui S, Mao S, Wen Z, Chang J, Zhang Y, Chen J. Controllable synthesis of silver nanoparticle-decorated reduced graphene oxide hybrids for ammonia detection. *Analyst*. 2013;138(10):2877-82.
26. Wang Y, Qiao Y, Chen Y, Hu T, Zhang L. One step pyrolysis synthesis of silver/nitrogen-doped carbon sheet for oxygen reduction in alkaline media. *International Journal of Hydrogen Energy*. 2017;42(36):22903-8.
27. Guo J, Hsu A, Chu D, Chen R. Improving oxygen reduction reaction activities on carbon-supported Ag nanoparticles in alkaline solutions. *The Journal of Physical Chemistry C*. 2010;114(10):4324-30.
28. Garcia AC, Gasparotto LHS, Gomes JF, Tremiliosi-Filho G. Straightforward Synthesis of Carbon-Supported Ag Nanoparticles and Their Application for the Oxygen Reduction Reaction. *Electrocatalysis*. 2012;3(2):147-52.
29. Masa J, Batchelor-McAuley C, Schuhmann W, Compton RG. Koutecky-Levich analysis applied to nanoparticle modified rotating disk electrodes: electrocatalysis or misinterpretation. *Nano Research*. 2014;7(1):71-8.
30. Chatenet M, Genies-Bultel L, Aurousseau M, Durand R, Andolfatto F. Oxygen reduction on silver catalysts in solutions containing various concentrations of sodium hydroxide – comparison with platinum. *Journal of Applied Electrochemistry*. 2002;32(10):1131-40.
31. Sheng Z-H, Shao L, Chen J-J, Bao W-J, Wang F-B, Xia X-H. Catalyst-Free Synthesis of Nitrogen-Doped Graphene via Thermal Annealing Graphite Oxide with Melamine and Its Excellent Electrocatalysis. *ACS Nano*. 2011;5(6):4350-8.
32. Yang T-H, Venkatesan S, Lien C-H, Chang J-L, Zen J-M. Nafion/lead oxide–manganese oxide combined catalyst for use as a highly efficient alkaline air electrode in zinc–air battery. *Electrochimica Acta*. 2011;56(17):6205-10.
33. Sumboja A, Ge X, Goh FWT, Li B, Geng D, Hor TSA, et al. Manganese Oxide Catalyst Grown on Carbon Paper as an Air Cathode for High-Performance Rechargeable Zinc–Air Batteries. *ChemPlusChem*. 2015;80(8):1341-6.



34. Li P-C, Hu C-C, Noda H, Habazaki H. Synthesis and characterization of carbon black/manganese oxide air cathodes for zinc–air batteries: Effects of the crystalline structure of manganese oxides. *Journal of Power Sources*. 2015;298:102-13.
35. Ma H, Wang B. A bifunctional electrocatalyst  $\alpha$ -MnO<sub>2</sub>-LaNiO<sub>3</sub>/carbon nanotube composite for rechargeable zinc–air batteries. *RSC Advances*. 2014;4(86):46084-92.
36. Çiplak Z, Yildiz N, Çalimli A. Investigation of Graphene/Ag Nanocomposites Synthesis Parameters for Two Different Synthesis Methods 2014. 361-70 p.
37. Vi TTT, Lue SJ. Preparation of silver nanoparticles loaded graphene oxide nanosheets for antibacterial activity. *IOP Conference Series: Materials Science and Engineering*. 2016;162(1):012033.
38. Sang S, Li D, Zhang H, Sun Y, Jian A, Zhang Q, et al. Facile synthesis of AgNPs on reduced graphene oxide for highly sensitive simultaneous detection of heavy metal ions. *RSC Advances*. 2017;7(35):21618-24.
39. Lilloja J, Kibena-Pöldsepp E, Merisalu M, Rauwel P, Matisen L, Niilisk A, et al. Supplementary Materials: An Oxygen Reduction Study of Graphene-Based Nanomaterials of Different Origin.
40. Neburchilov V, Wang H, Martin JJ, Qu W. A review on air cathodes for zinc–air fuel cells. *Journal of Power Sources*. 2010;195(5):1271-91.
41. Lee JS, Tai Kim S, Cao R, Choi NS, Liu M, Lee KT, et al. Metal–air batteries with high energy density: Li–air versus Zn–air. *Advanced Energy Materials*. 2011;1(1):34-50.
42. Geng D, Chen Y, Chen Y, Li Y, Li R, Sun X, et al. High oxygen-reduction activity and durability of nitrogen-doped graphene. *Energy & Environmental Science*. 2011;4(3):760-4.
43. Lima FH, Calegaro ML, Ticianelli EA. Investigations of the catalytic properties of manganese oxides for the oxygen reduction reaction in alkaline media. *Journal of Electroanalytical Chemistry*. 2006;590(2):152-60.



จุฬาลงกรณ์มหาวิทยาลัย  
**CHULALONGKORN UNIVERSITY**

## REFERENCES



จุฬาลงกรณ์มหาวิทยาลัย  
**CHULALONGKORN UNIVERSITY**



จุฬาลงกรณ์มหาวิทยาลัย  
**CHULALONGKORN UNIVERSITY**

**VITA**

**NAME** Laksanaporn Poolnapol

**DATE OF BIRTH** 08 July 1992

**PLACE OF BIRTH** Somdej Phra Boromma Ratchathewi Na Si Racha Hospital

**INSTITUTIONS ATTENDED** Chonkanyanukoon school  
King Mongkut's Institute of Technology Ladkrabang  
Chulalongkorn University

**HOME ADDRESS** 49/69 M.9 Bangpha Sriracha Chonburi 20110

**PUBLICATION** DEVELOPMENT ELECTROCATALYSTS SILVER DECORATED  
ON REDUCED GRAPHENE OXIDE FOR OXYGEN REDUCTION  
ZINC AIR BATTERY